NASA Contractor Report 178367

Application of Ray Theory to Propagation of Low Frequency Noise from Wind Turbines

James A. Hawkins

APPLIED RESEARCH LABORATORIES
THE UNIVERSITY OF TEXAS AT AUSTIN
POST OFFICE BOX 8029, AUSTIN, TEXAS 78713-8029

NASA

National Aeronautics and
Space Administration

Langley Research Center
Hampton, Virginia 23665-5225

NASA CONTRACTOR REPORT

NASA CR-178367

ARL-TR-87-40

APPLICATION OF RAY THEORY TO PROPAGATION OF LOW FREQUENCY NOISE FROM WIND TURBINES

FINAL REPORT UNDER CONTRACT NAS1-17802
20 July 1984 - 31 October 1987

James A. Hawkins

APPLIED RESEARCH LABORATORIES
THE UNIVERSITY OF TEXAS AT AUSTIN
POST OFFICE BOX 8029, AUSTIN, TEXAS 78713-8029

July 1987

Final Report

Prepared for:

NATIONAL AERONAUTICS AND SPACE ADMINISTRATION
LANGLEY RESEARCH CENTER
HAMPTON, VA   23665

NASA

National Aeronautics and
Space Administration

Langley Research Center
Hampton, Virginia 23665-5225

FOREWORD

This report is adapted from the master's thesis of the same title by James A. Hawkins. Soon after enrolling in the Department of Physics in 1984, Mr. Hawkins began work on the wind turbine noise propagation project. The date of his M.S. degree is December 1987. Professor C. W. Horton, Sr., was the second reader of the thesis.

The research was carried out at Applied Research Laboratories, The University of Texas at Austin. Appreciation is extended to the following persons for their assistance on the project. At Applied Research Laboratories A. J. Kimbrough carried out computing tasks of all kinds, T. L. Foreman gave counsel and advice on the use of his program MEDUSA, and E. K. Westwood helped with the beam displacement calculations. At NASA Langley Research Center W. L. Willshire, Jr., provided detailed information about the NASA data and made it possible for Mr. Hawkins to be present at the May-June 1985 tests at Medicine Bow, Wyoming; J. S. Preisser provided advice and support throughout the project.

Oral reports of the research have been given,[1,2] or are scheduled to be

---

[1]J. A. Hawkins, Jr., and David. T. Blackstock, "Propagation of noise from wind turbines," *Bull. Am. Phy. Soc.* **32**, 1179 (A) (1987).

[2]J. A. Hawkins, Jr., and David. T. Blackstock, "Application of ray theory to downwind propagation of low-frequency noise in the atmosphere," *J. Acoust. Soc. Am.* **79**, S19 (A) (1986).

given.[3] Support for the work came from NASA Langley Research Center under Contract NAS1–17802. Technical monitors were J. S. Preisser and W. L. Willshire, Jr.

David T. Blackstock,
Supervisor

---

[3]J. A. Hawkins and David. T. Blackstock, "Application of ray theory to propagation of low-frequency noise from wind turbines," *J. Acoust. Soc. Am.* **82**, S77 (A) (1987).

TABLE OF CONTENTS

LIST OF FIGURES

viii

CHAPTER 1

INTRODUCTION

1.1 Background

After the Arab oil embargo in the mid 70's, the United States increased its efforts to develop alternative energy sources. These sources included wind turbines. Because of advances in technology [1], it had become possible to build very large and powerful wind turbines. In fact, interest in wind turbine technology led to a variety of machine designs, the most practical of which make use of either a vertical or horizontal axis. A good example of a vertical axis machine is the Darrieus turbine, which is described in Ref. 1 as an 'eggbeater standing on end'. The horizontal axis machines have, as the name indicates, the wind turbine shaft mounted horizontally. Turbines are further classified as either upwind or downwind turbines. The blades of an upwind machine are upwind of the support tower, whereas the blades of a downwind machine are downwind of the support tower [2]. The common windmill is a good example of an upwind machine. A downwind turbine can be thought of as a backward facing windmill. Good examples of each type of turbine are described in Ref. 2.

In the fall of 1979 an unanticipated problem arose during initial testing of the MOD-1 turbine at Knob Hill, North Carolina, which was the largest downwind

turbine at that time [3]. It was discovered that the MOD-1 machine produced an annoying low frequency *thump* which was audible to people living within a radius of several kilometers.

Because of complaints directed at the MOD-1 turbine, interest developed in the noise produced by wind turbines [3]. The resulting investigations took two paths: environmental and scientific. The noise levels of the wind turbines were environmentally unacceptable, and thus would jeopardize community acceptance of more turbines (some of which were to be even larger than the MOD-1 machine). Therefore, early investigations were aimed at reducing the noise; in the case of the MOD-1 machine, the problem was solved by lowering the rotation rate. At the same time, large downwind turbines have received scientific interest because they are effective sources of low frequency noise, and in some cases their location proves ideal for propagation studies. For example, the WTS-4 turbine, which plays a central role in this investigation, is located in a relatively isolated flat area (i.e., a flat plane). Noise is produced well below 100 Hz; it is audible up to about 3 km and can be detected with instrumentation out to a range of 20 km.

1.2 Purpose of Work

Initially our goal in this investigation was to provide a general theoretical description of the propagation of noise from large wind turbines, in particular, the thumping noise produced by large downwind-type machines. The following aspects of the problem were to be investigated.

- Spherical spreading and directivity of the source

- Refraction due to wind and temperature gradients

- Ground effects

2

- Atmospheric absorption

- Turbulence[1]

However, in the fall of 1984 W. L. Willshire conducted preliminary experiments to measure the downwind propagation of noise from the WTS-4 wind turbine at the Department of Energy test site at Medicine Bow, Wyoming [5]. When Willshire's data became availabile, our goal became more focused. We wished to develop an accurate, effective theoretical model of *downwind propagation of low frequency noise* from wind turbines. Specifically, we wanted to be able to explain Willshire's 1984 data. Furthermore, Willshire carried out more elaborate experiments at the WTS-4 site the following year (May-June 1985). The model arrived at through investigation of the 1984 data was then to be tested against the May-June 1985 experiments.

1.3 Possible Approaches

After analyzing the 1984 data, Willshire initially believed that he had discovered an instance where the so-called *ground wave* (see Appendix A) is the predominant factor in sound propagation. Upon further investigation, he concluded that the predicted sound levels based solely on the contribution of the ground wave fell far below the measured levels [5]. Following Willshire's experiments, other investigations were undertaken, the purpose of which was to explain Willshire's 1984 data. In this section, we cite three investigations which illustrate the different approaches taken.

---

[1]To keep the scope of the investigation within acceptable limits, it was early decided not to investigate the role played by turbulence. A good review of turbulence effects can be found in Piercy's review [4].

Analytical investigations of sound propagation in an inhomogeneneous medium, say the ocean or the atmosphere, are usually based on *normal mode theory, the parabolic approximation,* or *ray theory.* Each theory has its strengths and weaknesses. In normal mode theory the acoustic wave equation is solved explicitly. A complete solution in normal modes is often prohibitively difficult, particularly in atmospheric acoustics. Nevertheless, valuable results have been obtained (see for example Chunchuzov [6]). Zorumski and Willshire [7], using the normal mode techniques of Chunchuzov, found good agreement between theory and data at receiver ranges far away from the turbine. But, since the application of normal mode theory to atmospheric noise propagation problems depends on being in the farfield [7], it cannot be used to study data near the source.

Although the parabolic approximation is used in ocean acoutics with good results [8], its use in atmospheric acoustics is relatively unknown. However, White [9], using the parabolic approximation, also obtained good agreement between theory and Willshire's 1984 data at long ranges. Again, however, predictions for near-source ranges were in question.

Because of the difficulties associated with normal mode theory (for example, the results obtained by Zorumski and Willshire are very complicated and difficult to interpret), ray theory is often employed as an alternative or as a first approximation to describing the sound field. Ray theory has the advantages of being easy to use and of providing a simple visualization of the sound field. However, because it is a high frequency approximation of the wave equation, ray theory also has limits of applicability. Furthermore, because ray theory ignores diffraction phenomena (for example, caustics), its application must be carefully evaluated. We have investigated simple ray theory, ray theory with *beam displacement,* and ray theory with *caustic corrections.* Because the problem we are

investigating involves very low frequencies and ray theory is generally considered a high frequency approximation, we expected ray theory to be of limited value. We found, however, that simple ray theory gives the most useful predictions of downwind noise levels of the WTS-4 wind turbine data. The success (at least for downwind propagation) of ray theory is encouraging from a practical standpoint because it is the simplest and easiest to use of all the competing theories. On the other hand, the application of ray theory to upwind data obtained in the 1985 tests proved to be nearly fruitless.

1.4 Atmospheric Acoustics

In this section we remind the reader of some simple concepts concerning refraction and reflection.[2] Our comments are based on Delany's review of the history of atmospheric acoustics [11]. Other good reviews can be found in the literature [4,12].

Throughout the history of atmospheric acoustics, accurate sound ranging has continually held the interest of investigators. Consider, for example, the boom of a cannon firing. If the speed of sound is known and the direction of the sound is known, then the position of the gun can be determined. An early achievement was the accurate determination of the speed of sound in air. Newton's derivation of the speed of sound together with Laplace's famous correction is well documented [13]. The speed of sound in air can be written in terms of the ratio of specific heats γ, the ambient pressure P, and the ambient density ρ,

$$c = \sqrt{\frac{\gamma P}{\rho}} \ . \tag{1.1}$$

---

[2]Although atmospheric absorption is important, it is negligible at the frequencies in which we are interested (see, for example, Ref. 10). Hence we shall not discuss it in this section.

Substitution of the perfect gas law $P = RT\rho$, where R is the gas constant and T is the absolute temperature, in Eq. (1.1) yields the sound speed in terms of the temperature

$$c = \sqrt{\gamma RT} \quad . \tag{1.2}$$

Successful sound ranging is complicated by the inhomogeneity of the atmosphere. Wind and temperature vary throughout with height and range, and the variation depends on the diurnal cycle. Furthermore, the variations can be coupled in the sense that variations in the wind can affect the temperature. The cumulative effect of wind and temperature variation is to bend, or *refract*, the sound waves. Thus, the 'line of sight' used in sound ranging is in fact not a straight line.[3]

As a conceptual device, we can introduce a curve tracing the path of sound propagation, i.e., a *ray* (for example, see section 5.13 of Ref. 14). Using the rule of thumb that rays curve so as to take the sound into a region of lower sound speed,[4] we can understand Fig. 1.1 (taken from Ref. 11). When the temperature decreases with height (normal *lapse* condition) as in Fig. 1.1(a), the rays bend upward. In Fig. 1.1(b) the temperature increases with height (temperature *inversion*), and the rays bend toward the ground. Note that when normal lapse

---

[3]Although refraction by wind and temperature gradients is well established today, it was not always so. In the 1870's, Tyndall and Henry carried out a historic debate concerning the propagation of sound in fog. The controversy concerned pecularities in the propagation of sound in a fog. For example, a ship sailing with the wind approaching a signaling station could not hear the station's foghorn, whereas the station could clearly hear the ship's bell. Another pecularity was the echo heard when a foghorn was sounded into apparently clear air. Tyndall contended that both pecularities of sound propagation were the result of *floculence* in the atmosphere. Although Tyndall never admitted it, Henry proved, by careful experimentation, that simple refraction caused sound sent upwind to go unheard. However, we know today that Henry's floculence is real and its study comes under the heading of scattering of sound by turbulence.

[4]Although this is not obvious, it can be derived from Snell's law $c_1/\cos\theta_1 = c_2/\cos\theta_2$, where the subscripts indicate the sound speed and angle of inclination of two points in the atmosphere (see, for example, pp. 401-402 in Ref. 14).

6
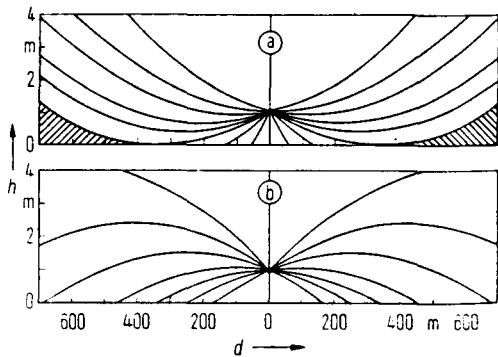
Figure 1.1 RAYS IN (A) A LAPSE CON-
DITION AND (B) AN INVERSION (FROM
REF. 11).
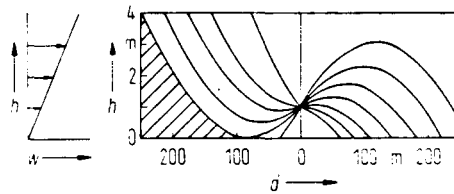
Figure 1.2 RAYS IN A WINDY ATMO-
SPHERE (FROM REF. 11).

conditions prevail a *shadow zone* forms (the shaded region of Fig. 1.1(A)). How-
ever, rays penetrate farther into the sound field in an inversion. At twilight on a
quiet evening, the atmosphere can change from a lapse condition to an inversion.
The change is sometimes cited as the reason that highway sounds can be heard
in certain locations at night but not during the day.

A similar situation arises for rays in a windy atmosphere, with an impor-
tant difference: wind produces a field of rays that is asymmetrical (see Fig. 1.2).
The propagation speed in a wind, directly upwind or downwind of the source, can
be written as the sum of the quiescent (no wind) sound speed c_0 and the wind
velocity w,

$$a = c_0 + w \quad , \tag{1.3}$$

where w is the contribution of the wind to the propagation speed. The com-
ponent of the wind velocity is added or subtracted, depending on whether the
receiver is downwind or upwind, respectively. If the wind velocity w increases
steadily with height, then the situation shown in Fig. 1.2 can be explained in the
following manner. Simply stated, the upwind propagation speed decreases with
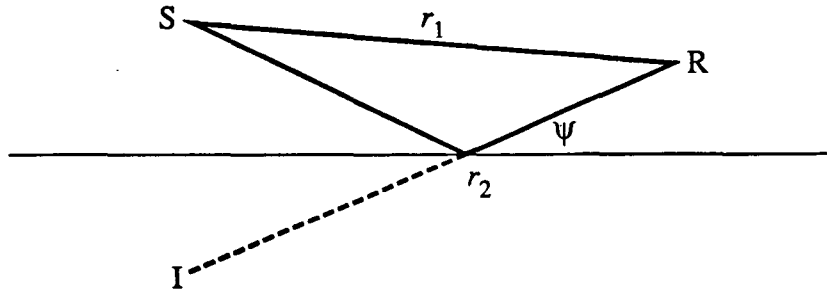
Figure 1.3 REFLECTION OF RAY FROM SOURCE NEAR A SURFACE.

height (i.e., the wind opposes the propagation of sound). Consequently the rays bend upward. Downwind, the propagation speed increases with height (the wind aids the propagation of sound) and the rays bend downward. In summary, we see that sound propagating upwind behaves as if a lapse condition existed, while sound propagating downwind behaves as if an inversion condition existed.

The ray picture of a sound field is simple and appealing.[5] It can give a good qualitative understanding of how sound propagates. Moreover, by means explained in Chapter 3, we can use ray theory to predict sound levels.

In Figs. 1.1 and 1.2 we have omitted reflected rays. However, their contribution to the sound field is particularly important. Delany writes that Derham [11] found that newly fallen snow weakened the propagation of sound and observed that the weakening disappeared when the ground became frozen solid. It is now known that the 'weakening' of sound propagation is due to absorption

---

[5]Although ray tracing is done now almost exclusively with computers, ray tracing is not limited to computers. For example, Rudnick [15] presents an analyses of rays in a refracting medium, and gives detailed instructions for use of a compass to draw rays by hand.

8

of sound by the ground. Consider the following expression (see Fig. 1.3),

$$\frac{p}{p_0} = (\frac{1}{r_1})e^{-ikr_1} + (\frac{R_p}{r_2})e^{-ikr_2} \quad , \tag{1.4}$$

where p_0 is the sound pressure at unit distance from the source S, p is the sound pressure at the receiver R, r_1 and r_2 are, respectively, the distances from the source and the image I [4]. The plane wave reflection coefficient R_p is defined as follows:

$$R_p = \frac{\sin \psi - (Z_1/Z_2)}{\sin \psi + (Z_1/Z_2)} \quad , \tag{1.5}$$

where Z_1 and Z_2 are the air impedance and ground impedance, respectively. Clearly, the weakening of sound by fresh snow in contrast to solid snow observed by Derham is caused by the smaller impedance of the fresh snow, which has a smaller reflection coefficient. The point to be made here is that complete and accurate results of long range propagation studies depend on the accurate specification of the reflection coefficient.

Note from Eq. (1.5) that when the source and the receiver are both very near the ground, or when they are a long way from each other, then $\psi \to 0$, $R_p \to -1$. When $R_p = -1$ the direct and reflected rays cancel, leaving a shadow zone. In fact, we have neglected to include a third term in Eq. (1.5). This term is negligible when ψ is *not* small, but it contributes to the sound field when ψ is small. The mechanism by which the contribution occurs is through the so-called *ground wave*. The ground wave is discussed in Appendix A. Ground wave effects, as we have previously mentioned, were studied by Willshire.

1.5 Scope of Topics and Results

The subject of this thesis is propagation, primarily downwind propagation, of low frequency noise from a downwind turbine. We have found that the

data measured by Willshire in 1984 and 1985 can be explained by using simple ray theory. Although we can include the effects of absorption by the ground, atmospheric absorption, and temperature variation, their effects have been found to be minimal compared to refraction by the wind gradient.

In the next chapter we describe the noise characteristics of the WTS-4 wind turbine. This information is gathered from reports by Willshire and others. A derivation of ray theory for a windy atmosphere and a short description of the computer program used to solve the ray equations are given in Chapter 3 (a more complete discussion of the computer program is the subject of Appendix C). Chapter 4 is about (1) the input data needed for MEDUSA and (2) the applications of MEDUSA most pertinent to our investigation. In Chapter 5 the ray theory predictions are compared with Willshire's 1984 data. The 1985 data, both upwind and downwind, are compared to ray theory predictions in Chapter 6. We summarize the results of our investigation and outline areas for future studies in Chapter 7. Additional topics covered in appendices include ground wave theory, beam displacement, caustics, and a short discussion of Willshire's mid-frequency measurements.

CHAPTER 2

NOISE PRODUCTION FROM THE WTS-4 WIND TURBINE

In Chapter 1 it was stated that the main goal of our investigation is to provide a method for predicting the downwind propagation of low frequency noise from large wind turbines. Of particular interest to our investigation are the data obtained by W. L. Willshire for the WTS-4 turbine at Medicine Bow, Wyoming, during September 1984 [5], and the follow-up experiments conducted during May-June 1985. We present in this chapter a brief general description of the WTS-4 machine, its noise characteristics, and the site. The emphasis is on the environmental parameters that must be specified and the assumptions that must be made in order to apply ray theory to the experiment. Much of the material in this section is drawn from reports by Willshire [5] and Shepherd and Hubbard [16].

2.1 Characteristics of the Turbine: Physical Dimensions and Overview of Operation

The WTS-4 turbine, shown in Fig. 2.1, is a twin-blade, horizontal-axis, downwind machine. Recall that "downwind" here that means the blade is downwind of the support tower. The nacelle at the top of the support tower houses
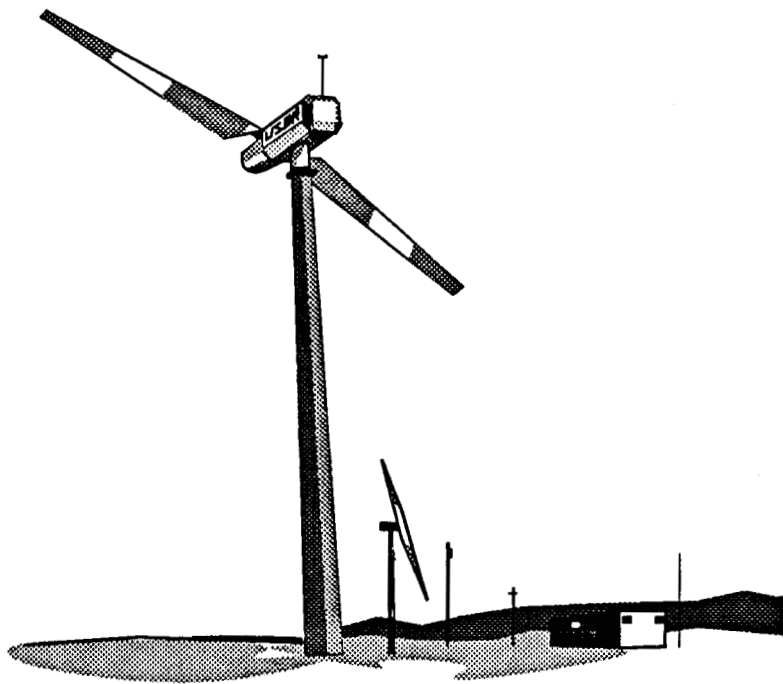
Figure 2.1 THE WTS-4 WIND TURBINE IN MEDICINE BOW, WYOMING (REDRAWN FROM REF. 5).
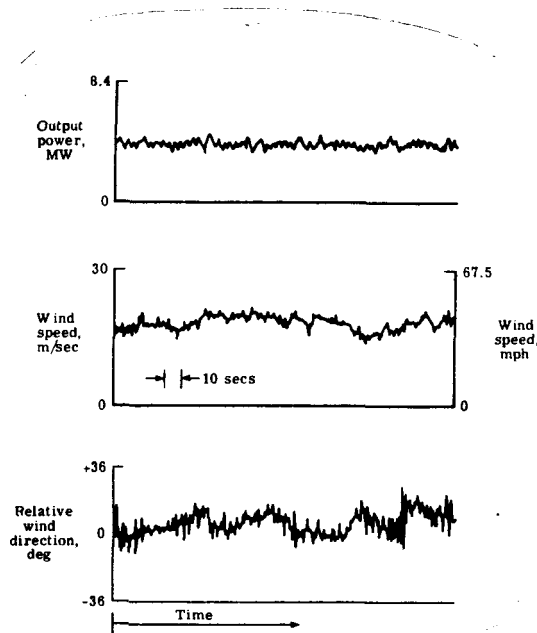
Figure 2.2 TYPICAL POWER OUTPUT, WIND DIRECTION, AND WIND VELOCITY (FROM REF. 16).

the electric generator. The blades are attached to the generator by the hub, the center of which is 80 m above ground level. The blades measure 80 m tip to tip. The highest point above the ground reached by a blade is 120 m, while the tip of the blade nearest the ground is 40 m from the ground.

The machine operates at a constant 30 rpm (hence the blade passage frequency is 1 Hz) and produces a maximum of 4.2 MW of electrical power. The cut-on and cut-off wind speeds—the wind speeds between which the turbine is designed to operate—are 7 m/s and 27 m/s (16 and 60 mph) respectively. The machine is maintained at a constant rpm in varying wind speeds by means of a trimming mechanism. Typical data on power output, wind direction, and wind velocity are shown in Fig. 2.2.

13

2.2 Atmospheric Conditions

Although the atmosphere measures some 500-600 km from the earth's surface to the edge of the interplanetary gas, the major weather patterns develop in the first 10 km [17]. Within the first 10 km, it is only the first few hundred meters above the ground which directly affect downwind sound propagation along the ground. We can get an idea of the height above which the atmosphere does not affect propagation by considering the *limiting* ray. Rays launched at angles greater than the limiting ray do not contribute to the sound field, but rays launched at lesser angles can contribute to the field. In Fig. 1.2 for example, of the seven downwind rays shown, only five contribute to the sound field out to 200 m. The highest point of the limiting ray defines a rough height above which the atmosphere has minimum effect on sound propagation. In our investigation, as we shall see (Chap. 4), this height is only a few hundred meters high.

Normally one expects all three important atmospheric conditions—temperature, humidity, and wind velocity—to vary with height in the region of the atmosphere near the ground (the first few hundred meters near the ground). Because the turbine operates in windy conditions, however, the atmosphere is well mixed when noise is radiated. The atmosphere is therefore assumed to have constant humidity and to be isothermal near the ground. The wind, on the other hand, does vary with height and it turns out that this variation has a very important effect on sound propagation.

2.3 Ground Characteristics

The turbine is located within a broad flat basin formed by the Laramie, Medicine Bow, and Shirley mountain ranges. The vegetation consists mostly of

14

small bushes and clumps of grass. No trees exist in the immediate vicinity of the turbine site. The dry, slightly sandy soil in the area is easily crumbled by hand.

The effect of the ground on the propagation of sound requires that the ground impedance be determined. We assume here that the ground can be characterized as a flat plane with a complex impedance. In our investigation the Delany and Bazley impedance model [18] as formulated by Chessel [19] is used (see Chapter 4).

2.4   General Description of Sound Source and Sound Field

The noise from downwind turbines is of two types. The first type is aerodynamic noise. Although this noise contributes a small amount at the low end of the acoustic spectrum, the main components are between 800 and 2500 Hz. This noise is generally thought to be caused by"unsteady airfoil loads ... and convection of the turbulent boundary layer past the trailing edge of the airfoil"[20].[1] Because the convection past the trailing edge increases with increasing wind velocity, the source of the high frequency sound is considered to be located near the top (120 m) of the turbine.

The second type of noise is primarily low frequency in character and is caused by the passage of the turbine blade through the turbulent wake of the support tower. The entire blade is subject to the impulsive aerodynamic loading changes as it passes through the wake; thus the sudden change in angle of attack of the blade produces a thump. Consequently the spectrum is rich in harmonics of the blade passage frequency (1 Hz). Figure 2.3 shows a representative time trace for the thumping noise, and Fig. 2.4 shows the low frequency portion of

---

[1]It appears now that the mechanism is more complicated than previously considered (see Ref. 21).
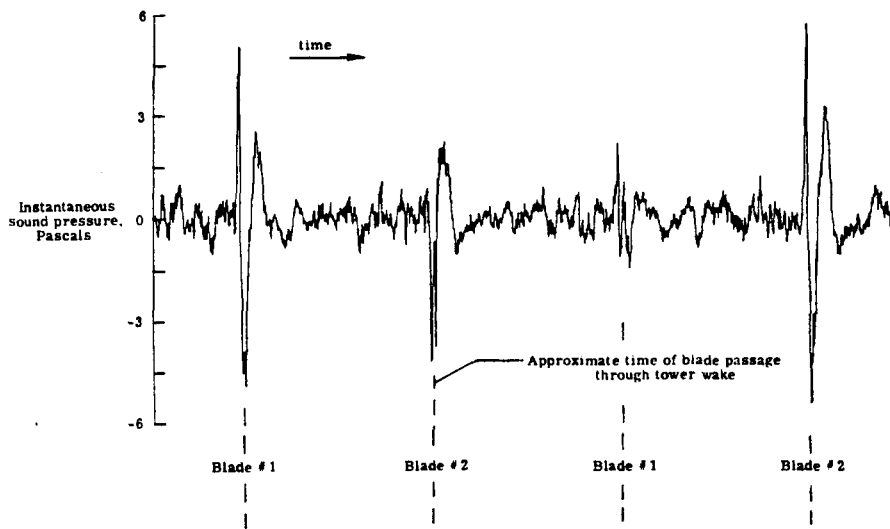
Figure 2.3 TIME HISTORY OF THE THUMPING NOISE (FROM REF. 16).

the noise spectrum for the WTS-4 machine. The low frequency components, in particular the region of the spectrum between 1 Hz and 20 Hz, are thought to be due primarily to the thump.

Because of the nature of the blade (thickest near its root, thinnest at its tip), the cantilever deflection is greatest at the tip. For simplicity, we assume that the vibrating surface (the sound source) is concentrated at the tip, in particular, the region from the tip to one chord width up the blade. We can gain an idea of how concentrated a source is by considering its compactness. A source is considered acoustically compact if the wavelengths of the sound produced are long in comparison with the principal dimension of the source. For compact sources the product of the wave number with the principal dimension must be less than one, $kl \ll 1$, where k is the wave number and l the principal dimension

16
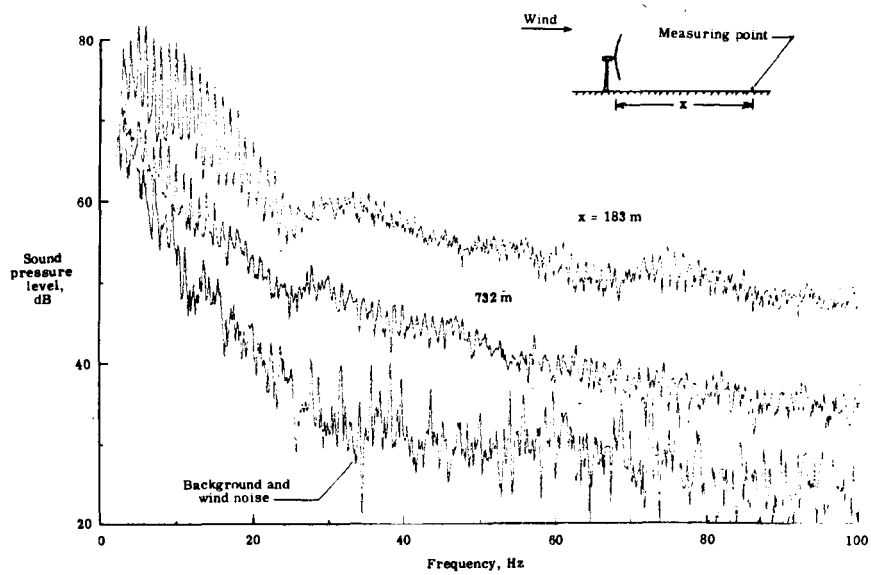
Figure 2.4 TYPICAL FREQUENCY SPECTRUM FOR THE THUMPING NOISE. NOTE THE STRONG COMPONENTS BETWEEN 1 Hz AND 20 Hz (FROM REF. 16).

17

of the source (for example, see Ref. 22, p. 25). Because the tip of the WTS-4 turbine blade undergoes the largest deflection as it passes through the tower wake, we can assume that a disc with a diameter of $l = 1.04$ m (the tip chord width) is the source. Consequently, the principal dimension is taken to be 1.04 m. At 1 Hz the product kl is

$$kl = \frac{2\pi}{c_0}(1.04) \approx .02$$

and at 100 Hz

$$kl = \frac{200\pi}{c_0}(1.04) \approx 2 \quad .$$

Hence, it is seen that for very low frequencies (1 Hz to 20 Hz) the source is relatively compact. The approximation becomes progressively worse for higher frequencies. In summary, we assume that the low frequency sound from the WTS-4 turbine is from a point source, which is located at the blade tip as it passes through the turbulent wake of the tower.

We comment on one other aspect of the sound field. Since it is considered to be a small disc approximately 1 m in diameter, the source is expected to exhibit dipole characteristics. Figure 2.5 shows a plan view of the WTS-4 turbine sound levels at two ranges, near the source (183 m) and at mid-range (732 m). At 183 m, along a line in the plane of blade rotation, the notch in the sound level at 90° is characteristice of dipole directivity. The dipole nature of the source is not of direct importance in our investigation, because our interest is in sound propagated either straight downwind or upwind.

In summary, the WTS-4 turbine can be thought of as an ideal model of a low frequency dipole sound source, and its site is a close approximation of a flat plane. In the next chapter, the theoretical framework needed to study the propagation of sound from the WTS-4 machine (ray theory for sound in a wind) is described.

18
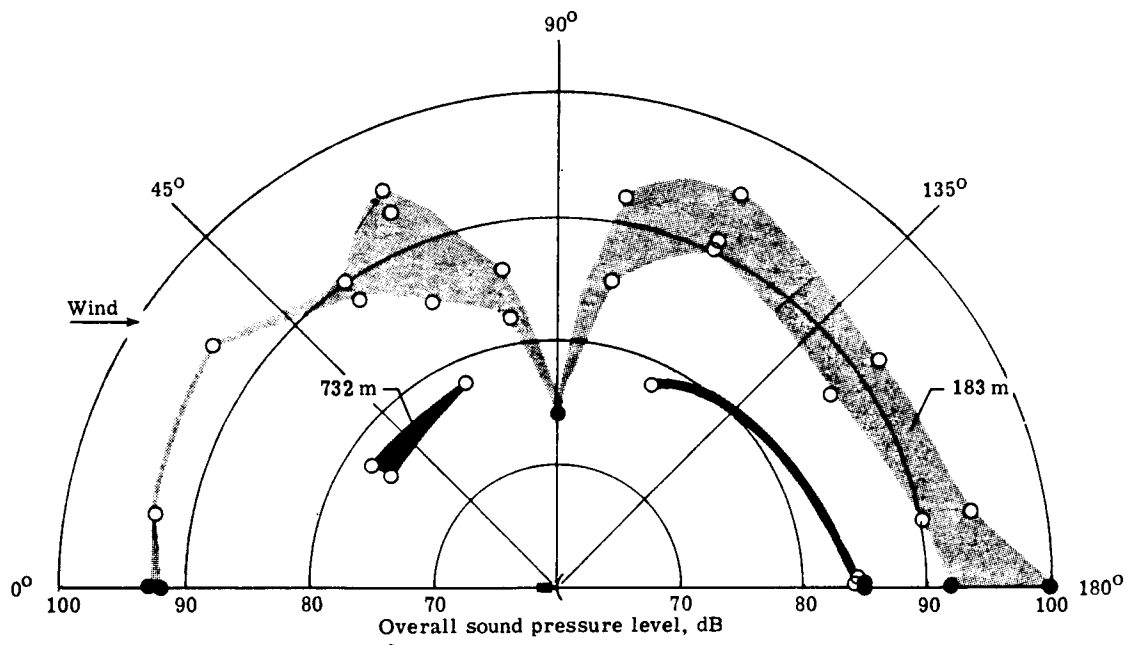
Figure 2.5 PLAN VIEW OF THE OVERALL SOUND PRESSURE LEVELS FOR THE WTS-4 WIND TURBINE (FROM REF. 16).

19

CHAPTER 3

RAY THEORY FOR SOUND IN A WIND

Ray theory for sound propagation in a windy atmosphere is developed in this chapter. First, the development of ray theory for a steady moving medium yields the general ray tracing equations. Introduced next are restrictions which specifically adapt these equations to a stratified, unidirectional moving medium, by which we mean that the medium velocity and sound speed vary only with height, and the medium is in motion in one direction. Assumptions are then made which tailor the resulting ray path equations to apply to sound propagation in the wind at the WTS-4 site. Finally, we briefly discuss the computer solution to the ray equation.

The idea of a ray path associated with the propagation of a wave is familiar. The ray path equation places this idea on firm ground, and the solution of the ray path equation allows the ray paths to be calculated. Moreover, the sound intensity along the ray path may be calculated and, subsequently, the propagation loss.

20

3.1 General Ray Theory for a Moving Medium

We want to investigate the effect of a moving medium on the propagation of sound waves. Sections 3.1 and 3.2 are based on the material in Chap. 8 of the text by A. D. Pierce (Ref. 10, Chap. 8). The goal here is not to explain in detail but simply to summarize results necessary for the development of ray theory.

First, we introduce the idea of a point located on a wavefront. A wavefront may be thought of as *a surface of constant phase*, which can be expressed at some time t and position $\mathbf{x}$ as $t = \tau(\mathbf{x})$. Consider a point P located at $\mathbf{x}_p(t)$ on an arbitrary wavefront $t = \tau(\mathbf{x})$ (see Fig. 3.1). The medium moves with velocity $\mathbf{w}$ without time variation. As time increases P traces a path in space. The velocity with which the point travels along the path is the vector sum of the wind velocity vector and the sound speed in the direction normal to the wavefront

$$\frac{d\mathbf{x}_p(t)}{dt} = \mathbf{w} + \hat{n}c = \mathbf{v}_{ray} \quad , \tag{3.1}$$

where c is the sound speed, $\hat{n}$ is the unit normal to the wave, and $\mathbf{w}$ is the the wind velocity. The solution $\mathbf{x}_p(t)$ of Eq. (3.1) defines the *ray paths*.

Note that in the case of a nonmoving medium we are concerned with the velocity at which the wavefront moves normal to itself, $\hat{n} \cdot \hat{n}c$, whereas for a moving medium we are concerned with the magnitude of the velocity of the point P, i.e., $|\mathbf{v}_{ray}| = |c\hat{n} + \mathbf{w}|$. The fact that the ray velocity has two components, one in the direction normal to the wavefront and another along the direction of the wind velocity, sometimes leads to confusion. For example, it is commonly said that Rayleigh missed the fact that the wave normal is not coincident with the ray velocity vector (see [11], pp. 210–212). However, when propagation is in the direction of the moving medium, the difference in direction between $\mathbf{v}_{ray}$ and $\hat{n}$
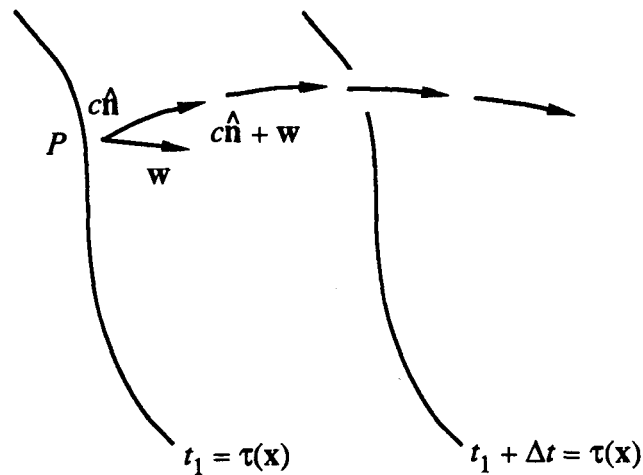
Figure 3.1 SCHEMATIC DIAGRAM SHOWING PROPAGATION OF A POINT P LOCATED ON A WAVEFRONT. THE WAVEFRONT AT TIME t_1 IS REPRESENTED BY THE CURVE $t_1 = \tau(\mathbf{x})$, AT A LATER TIME $t_1 + \Delta t$ BY THE CURVE $t_1 + \Delta t = \tau(\mathbf{x})$. THE ASSOCIATED SOUND SPEED NORMAL IS $c\hat{\mathbf{n}}$, THE WIND VELOCITY VECTOR IS $\mathbf{w}$, AND THE RAY VELOCITY VECTOR IS $\mathbf{v}_{ray} = c\hat{\mathbf{n}} + \mathbf{w}$.

is small.

The solution of Eq. (3.1) proves to be difficult to obtain because it requires knowledge of $\hat{\mathbf{n}}$ as a function of time t. The difficulty is avoided by the introduction of the so-called slowness vector $\nabla\tau$. The slowness vector is the gradient of the wavefront surface, which is in same direction as $\hat{\mathbf{n}}$. The equation for the slowness vector (see Ref. 10, Eq. (8-1.3)) is

$$\hat{\mathbf{n}} = \frac{c\nabla\tau}{\Omega} \quad , \tag{3.2}$$

where $\Omega = (1 - \mathbf{w} \cdot \nabla\tau)$. If Eq. (3.2) is squared and rearranged, the *eikonal equation*,

$$|\nabla\tau|^2 = \frac{\Omega^2}{c^2} \quad , \tag{3.3}$$

is obtained. The eikonal equation and the slowness vector are essential to the

22

derivation of the ray equations, the development of which is the subject of the next section.

3.2 General Ray Equations for a Moving Medium

Two equations are necessary in order to completely specify the ray path $\mathbf{x}(t)$ (the subscript p is dropped hereafter). The first equation is obtained simply by subtituting Eq. (3.2) into Eq. (3.1)

$$\frac{d\mathbf{x}}{dt} = \frac{c^2}{\Omega}\nabla\tau + \mathbf{w} \quad . \tag{3.4}$$

The second is obtained by explicitly differentiating the slowness vector

$$\begin{aligned}\frac{d}{dt}\nabla\tau &= \left(\frac{d\mathbf{x}}{dt}\cdot\frac{d}{d\mathbf{x}}\right)\nabla\tau \\ &= \left(\frac{d\mathbf{x}}{dt}\cdot\nabla\right)\nabla\tau \quad . \end{aligned} \tag{3.5}$$

Substitution of Eq. (3.1) for $d\mathbf{x}/dt$ in Eq. (3.5) yields

$$\begin{aligned}\frac{d}{dt}\nabla\tau &= \left[(c\hat{\mathbf{n}}+\mathbf{w})\cdot\nabla\right]\nabla\tau \\ &= c\left(\hat{\mathbf{n}}\cdot\nabla\right)\nabla\tau + (\mathbf{w}\cdot\nabla)\nabla\tau \quad . \end{aligned} \tag{3.6}$$

Substituting Eq. (3.2) for $\hat{\mathbf{n}}$, we can write Eq. (3.6) as

$$\frac{d}{dt}\nabla\tau = \frac{c^2}{\Omega}\left(\nabla\tau\cdot\nabla\right)\nabla\tau + (\mathbf{w}\cdot\nabla)\nabla\tau \quad . \tag{3.7}$$

Use of a vector identity for the first term on the right side of Eq. (3.7) leads to

$$\begin{aligned}\frac{d}{dt}\nabla\tau &= \frac{c^2}{\Omega}\frac{1}{2}\left(\nabla\left(|\nabla\tau|^2\right)\right) - \nabla\tau\times(\nabla\times\nabla\tau) + (\mathbf{w}\cdot\nabla)\nabla\tau \\ &= \frac{c^2}{\Omega}\frac{1}{2}\left(\nabla\left(|\nabla\tau|^2\right)\right) + (\mathbf{w}\cdot\nabla)\nabla\tau \quad , \end{aligned} \tag{3.8}$$

where the fact that the curl of the gradient is zero ($\nabla \times \nabla \tau = 0$) has been used. Using the formula for the eikonal Eq. (3.3) and taking the gradient, we can write Eq. (3.8) as

$$
\begin{aligned}
\frac{d}{dt}\nabla\tau &= \frac{c^2}{\Omega}\frac{1}{2}\left[\nabla\left(\frac{\Omega^2}{c^2}\right)\right] + (\mathbf{w}\cdot\nabla)\nabla\tau \\
&= -\frac{\Omega}{c}\nabla c + \nabla\Omega + (\mathbf{w}\cdot\nabla)\nabla\tau \\
&= -\frac{\Omega}{c}\nabla c + \nabla(1 - \mathbf{w}\cdot\nabla\tau) + (\mathbf{w}\cdot\nabla)\nabla\tau \quad , \qquad (3.9)
\end{aligned}
$$

where the definition $\Omega = (1 - \mathbf{w}\cdot\nabla\tau)$ has been used. Use of another vector identity allows us to write the third term of Eq. (3.9) as

$$
\begin{aligned}
\nabla(\mathbf{w}\cdot\nabla) &= (\nabla\tau\cdot\nabla)\mathbf{w} + (\mathbf{w}\cdot\nabla)\nabla\tau + \nabla\tau\times(\nabla\times\mathbf{w}) \\
&\quad + \mathbf{w}\times(\nabla\times\nabla\tau) \\
&= (\nabla\tau\cdot\nabla)\mathbf{w} + (\mathbf{w}\cdot\nabla)\nabla\tau + \nabla\tau\times(\nabla\times\mathbf{w}) \quad . \quad (3.10)
\end{aligned}
$$

Equation (3.9), with the substitution for $(\mathbf{w}\cdot\nabla)\nabla\tau$ from Eq. (3.10), is now written as

$$
\frac{d}{dt}\nabla\tau = -\frac{\Omega}{c}\nabla c - \nabla\tau\times(\nabla\times\mathbf{w}) - (\nabla\tau\cdot\nabla)\mathbf{w} \quad . \qquad (3.11)
$$

Equation (3.11) is the form sought for the time rate of change of the slowness vector, and is second of the two equations needed for the derivation of the ray paths. At this point the only restriction placed on the medium is that it moves steadily, that is, without time variation.

Equations (3.11) and (3.4) are the *ray equations* or *ray tracing* equations. The solution $\mathbf{x}(t)$ gives the equation for the ray paths. We introduce restrictions in the next section which tailor the ray equations for application to a medium where the wind $\mathbf{w}$ and sound speed c vary only with height.

24

3.3 The Special Case of Downwind Propagation

We can impose two restrictions which simplify the ray equations Eqs. (3.11) and (3.4). First, we restrict ourselves to *downwind propagation* so that the normal to the wavefront $\hat{n}$ has only height and range components. Consequently, the slowness vector $\nabla\tau$ can be written

$$\nabla\tau = \frac{\partial\tau}{\partial r}\hat{r} + \frac{\partial\tau}{\partial z}\hat{z} \quad ,$$

where $\hat{r}$ and $\hat{z}$ are unit vectors in the direction of range and height, respectively. Second, we assume that the wind and sound speeds vary only with height so that they can be written as

$$\mathbf{w} = w(z)\hat{r} \quad \text{and} \quad c = c(z) \quad .$$

Under these restrictions, the second and third terms of Eq. (3.11) can be combined as

$$
\begin{aligned}
-\nabla\tau \times (\nabla \times \mathbf{w}) - (\nabla\tau \cdot \nabla)\mathbf{w} &= -\begin{vmatrix} \hat{r} & \hat{y} & \hat{z} \\ \frac{\partial\tau}{\partial z} & 0 & \frac{\partial\tau}{\partial z} \\ 0 & \frac{\partial w}{\partial z} & 0 \end{vmatrix} - \frac{\partial\tau}{\partial z}\frac{\partial w}{\partial z}\hat{r} \\
&= \frac{\partial\tau}{\partial z}\frac{\partial w}{\partial z}\hat{r} - \frac{\partial\tau}{\partial r}\frac{\partial w}{\partial z}\hat{z} - \frac{\partial\tau}{\partial z}\frac{\partial w}{\partial z}\hat{r} \\
&= -\frac{\partial\tau}{\partial r}\frac{\partial w}{\partial z}\hat{z} \quad , \qquad (3.12)
\end{aligned}
$$

where $\hat{y}$ is the unit vector in the direction normal to both $\hat{r}$ and $\hat{z}$.

The range components of the ray equations, Eqs. (3.11) and (3.4), can now be written as

$$\frac{d}{dt}\frac{\partial\tau}{\partial r} = 0 \qquad (3.13)$$

and

$$\frac{dr}{dt} = \frac{c^2}{\Omega}\frac{\partial\tau}{\partial r} + w \quad , \qquad (3.14)$$

respectively. Similarly, the height components of the ray equations are

$$\frac{d}{dt}\frac{\partial \tau}{\partial z} = -\frac{\Omega}{c}\frac{dc}{dz} - \frac{\partial \tau}{\partial z}\frac{dw}{dz} \qquad (3.15)$$

and

$$\frac{dz}{dt} = \frac{c^2}{\Omega}\frac{\partial \tau}{\partial z} \quad , \qquad (3.16)$$

respectively.

We now eliminate time from the ray equations to obtain a differential equation for the coordinates, z and r, of the ray. The substitution of $\partial \tau / \partial z$ from Eq. (3.16) into Eq (3.15) yields

$$\frac{d}{dt}\left(\frac{\Omega}{c^2}\frac{dz}{dt}\right) = -\frac{\Omega}{c}\frac{dc}{dz} - \frac{\partial \tau}{\partial z}\frac{dw}{dz} \quad . \qquad (3.17)$$

An element of length along the ray path is defined as $dl = U dt$, where

$$U = |\mathbf{v}_{ray}| = |\mathbf{w} + c\hat{n}| \qquad (3.18)$$

is the magnitude of the ray velocity. Substitution of $U^{-1}dl$ for dt in Eq. (3.17) yields

$$U\frac{d}{dl}\left(\frac{\Omega}{c^2}U\frac{dz}{dl}\right) = -\frac{\Omega}{c}\frac{dc}{dz} - \frac{\partial \tau}{\partial z}\frac{dw}{dz} \quad . \qquad (3.19)$$

Given the relation $d/dl = \cos\theta \, d/dr$ (see Fig. 3.2), Eq. (3.19) can be written as

$$\cos^2\theta \frac{d^2z}{dr^2} = -\frac{c}{U^2}\frac{dc}{dz} - \frac{c^2}{\Omega U^2}\frac{\partial \tau}{\partial z}\frac{dw}{dz} \qquad (3.20)$$

or as

$$\frac{d^2z}{dr^2} = \left[1 + \left(\frac{dz}{dr}\right)^2\right]\left(\frac{c}{U}\right)^2\left(-\frac{1}{c}\frac{dc}{dz} - \frac{1}{\Omega}\frac{\partial \tau}{\partial r}\frac{dw}{dz}\right) \quad , \qquad (3.21)$$

where we have substituted

$$\cos^2\theta = \frac{1}{\sqrt{1 + (\frac{dz}{dr})^2}} \quad .$$

26
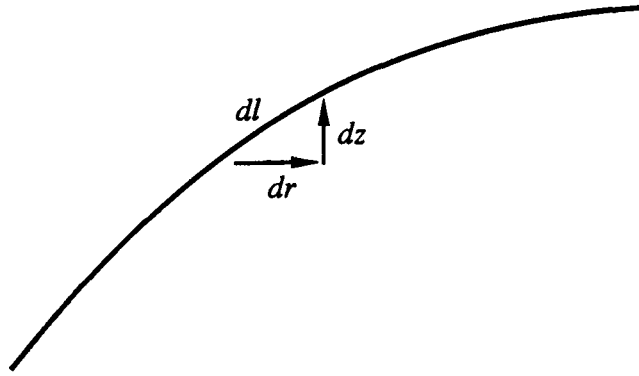
Figure 3.2 RELATIONSHIP OF AN ELEMENT OF RAY PATH LENGTH dl TO ELEMENTS OF RANGE dr AND HEIGHT dz.

It can immediately be seen from Eq. (3.13) that the radial component of $\nabla\tau$, $\partial\tau/\partial r$ is constant with respect to time. Furthermore, $\partial\tau/\partial r$ can be written as

$$
\begin{aligned}
\frac{\partial\tau}{\partial r} &= \nabla\tau\cdot\hat{\mathbf{r}} \\
&= \frac{\Omega}{c}\hat{\mathbf{n}}\cdot\hat{\mathbf{r}} \\
&= \Omega\frac{\cos\theta}{c} \quad,
\end{aligned}
\tag{3.22}
$$

where Eq. (3.2) has been substituted for $\nabla\tau$. Equation (3.22) is Snell's law for sound waves in a moving medium. Substitution of Eq. (3.22) in Eq. (3.21) yields

$$
\frac{d^2z}{dr^2} = \left[1 + \left(\frac{dz}{dr}\right)^2\right]\left(\frac{c}{U}\right)^2\left(\frac{1}{c}\frac{dc}{dz} - \frac{\cos\theta}{c}\frac{dw}{dz}\right) \quad.
\tag{3.23}
$$

Given the initial position and slope of a ray, we can locate the ray at any field point by solving Eq. (3.23). Consequently, Eq. (3.23) may be called the ray path equation. Note in Eq. (3.23) that the variation of the wind enters the equation explicitly as the term dw/dz . Variations in the sound speed c (for

example, the variation of c with temperature) can be accounted for through the term dc/dz.

Recall that we have invoked two restrictions in obtaining the ray path equation, Eq. (3.23).[1] First, we consider sound propagation only directly downwind of the source. This presupposes that the wind is blowing, without time variation, in a single direction. Second, we assume that the wind and the sound speed vary only with the height above the ground.

3.4   Numerical Solution: MEDUSA

Equation (3.23) is a second order nonlinear differential equation, the solution of which can be obtained by standard computer implemented numerical techniques. Rather than 'reinvent the wheel' by designing a program to numerically solve Eq. (3.23), we have chosen to adapt an existing program, MEDUSA [23], designed by T. L. Foreman of Applied Research Laboratories, The University of Texas at Austin. MEDUSA uses a third order Runge-Kutta algorithm with variable step size to numerically solve the ray path equation.

MEDUSA was chosen because it is powerful and reliable (Appendix C). In fact, MEDUSA has the unique capability to account for a range variable environment, for example, a sloping ocean bottom and a sound speed which varies with range; however, we did not have an opportunity to exploit this feature. More important to our investigation is that MEDUSA has proved easily adaptable for use in the study of downwind propagation of sound. Nevertheless, MEDUSA was designed for the study of underwater sound. That is, MEDUSA deals with an

---

[1]Although we have not previously stated the assumptions underlying the theory outlined in Sec. 3.1, we note here that the basic theory "tacitly assumes that the amplitude varies only slightly over distances comparable to a wavelength and that the radii of curvature of the wavefront are substantially larger than a wavelength" (see Ref. 10, Chap. 8).

environment which varies with *depth* and range (an ocean, for example) and does *not* vary in the azimuthal direction. Consequently, we must keep in mind that we are restricted to studying sound propagation in the downwind direction.

The adaptation of MEDUSA to our investigation is straightforward. Nevertheless, MEDUSA was designed for an underwater environment . Consequently, two problems must be resolved. First, we have to create the model of an ocean which has the environmental properties of the atmosphere. In the model, ground properties are substituted for ocean bottom properties and atmospheric properties are substituted for ocean properties. Furthermore, the ocean bottom is made very deep. This assures us that surface reflected rays do not affect the portion of the sound field in which we are interested. For example, in our investigation we have placed the ocean bottom at 1000 m, the sound source at 960 m, and the receiver at 999.5 m. Translating these distances to height above the ground, we see that the 'surface' of the atmosphere is 1000 m, the source 40 m above the ground, and the receiver is 0.5 m above the ground. In Section 4.1 we discuss in detail the construction of an ocean which models the atmosphere.

The second problem is the difference between the ray path equation for a non-moving nonhomogeneous static medium, the ocean, and for a moving non-homogeneous medium, the atmosphere. The problem is resolved by constructing a sound speed profile that is acceptable to MEDUSA and yet describes the propagation speed variation appropriate for a windy atmosphere. In the following we show that the choice of an appropriate sound speed profile adapts MEDUSA to the study of downwind propagation of sound.

The ray equation used with MEDUSA (see Ref. 23, Eq. (II.21)) is

$$\frac{d^2z}{dr^2} = \left[1 + \left(\frac{dz}{dr}\right)^2\right]\left(\frac{1}{n}\frac{\partial n}{\partial z} - \frac{dz}{dr}\frac{1}{n}\frac{\partial n}{\partial r}\right) \quad , \qquad (3.24)$$

where $n = c_{ref}/c$ is the acoustic index of refraction and c_{ref} is a suitable reference sound speed. If we assume the total propagation speed in the downwind direction is given by the sum of the static, *iosthermal* sound speed c_0 $(dc_0/dz = 0)$ and the component of the magnitude of the wind velocity w in the direction of propagation, then the total propagation speed is

$$a = c_0 + w \cos \theta \quad , \tag{3.25}$$

and because c_{ref} is a constant, the index of refraction can be written

$$n = \frac{1}{a} = \frac{1}{c_0 + w \cos \theta} \quad , \tag{3.26}$$

where $w = w(z)$ only and c_0 is independent of range and height. Therefore, Eq. (3.24) becomes

$$
\begin{aligned}
\frac{d^2 z}{dr^2} &= \left[1 + \left(\frac{dz}{dr} \right)^2 \right] \left[a \frac{d}{dz} \left(\frac{1}{a} \right) \right] \\
&= \left[1 + \left(\frac{dz}{dr} \right)^2 \right] \left(-\frac{1}{a} \frac{da}{dz} \right) \\
&= \left[1 + \left(\frac{dz}{dr} \right)^2 \right] \left(-\frac{1}{c_0 + w \cos \theta} \frac{d \left(c_0 + w \cos \theta \right)}{dz} \right) \quad . \tag{3.27}
\end{aligned}
$$

The term $\partial n / \partial r$ in Eq. (3.24) is discarded because the sound speed is assumed not to vary with range. If $\cos \theta \simeq 1$, then Eq. (3.27) becomes

$$\left[1 + \left(\frac{dz}{dr} \right)^2 \right] \left[-\frac{1}{c_0 + w} \frac{dw}{dz} \right] \quad . \tag{3.28}$$

where we have used $dc_0/dz = 0$.

Now consider Eq. (3.23), in which c is the isothermal sound speed, $c = c_0$. Therefore $dc_0/dz = 0$ and Eq. (3.23) can be written as

$$\frac{d^2 z}{dr^2} = \left[1 + \left(\frac{dz}{dr} \right)^2 \right] \left(\frac{c_0}{U} \right)^2 \left(-\frac{\cos \theta}{c_0} \frac{dw}{dz} \right) \quad . \tag{3.29}$$

The square of the magnitude of the ray velocity Eq. (3.28) is written as

$$
\begin{aligned}
U^2 &= (\mathbf{w} + c_0\hat{\mathbf{n}}) \cdot (\mathbf{w} + c_0\hat{\mathbf{n}}) \\
&= w^2 + 2c_0\mathbf{w} \cdot \hat{\mathbf{n}} + \left(\frac{w}{c_0}\right)^2 \\
&= w^2 + 2c_0 w \cos\theta + \left(\frac{w}{c_0}\right)^2 \quad .
\end{aligned}
\tag{3.30}
$$

Therefore, we can write

$$
\begin{aligned}
\left(\frac{c_0}{U}\right)^2 &= \frac{1}{1 + 2\left(\frac{w}{c_0}\cos\theta\right) + \left(\frac{w}{c_0}\right)^2} \\
&= 1 - 2\left(\frac{w}{c_0}\cos\theta\right) + \dots \quad .
\end{aligned}
\tag{3.31}
$$

Furthermore, if we assume $w \ll c_0$, then

$$
\left(\frac{c_0}{U}\right)^2 \simeq 1 \quad .
\tag{3.32}
$$

Therefore, Eq. (3.29) becomes

$$
\frac{d^2 z}{dr^2} = \left[1 + \left(\frac{dz}{dr}\right)^2\right]\left(-\frac{\cos\theta}{c_0}\frac{dw}{dz}\right) \quad .
\tag{3.33}
$$

Comparison of Eq. (3.28) and Eq. (3.33) reveals that the two ray equations are equivalent under the following conditions:

- $w \ll c_0$

- $\cos\theta \simeq 1$.

The first condition $w \ll c_0$ is easily met. At the WTS-4 wind turbine site, the wind speed is on the order of 10 m/s whereas the static sound speed in air at 20°C is 343 m/s. The second condition, $\cos\theta \simeq 1$, occurs when the rays are nearly parallel to the ground. In fact, it turns out that the most important rays

are those which propagate nearly parallel to the ground and the approximation $\cos(\theta) \simeq 1$ is a good one. The predominance of these rays will be demonstrated in Chapter 4, in which the environmental model and applications of the computer implemented numerical solution of Eq. (3.5) are discussed.

32

CHAPTER 4

USE OF THE RAY THEORY PROGRAM MEDUSA

The derivation of the ray path equation, Eq. (3.12), is described in Chapter 3. In this chapter we construct a model that adequately describes the WTS-4 turbine and site and describe pertinent applications of the computer program MEDUSA. To run MEDUSA an input data file must be created that contains the following data: *sound speed profile, sound source location, receiver height, frequency, atmospheric absorption,* and *ground impedance.* If an analytical expression for an environmental input parameter is known, it may be incorporated in MEDUSA as a separate subroutine. After the data file is created, the application programs can be run. We have used the application programs to calculate the following: *ray paths, propagation loss,* and *location of caustics.* We now discuss in greater detail the environmental properties which constitute the input data and the applications.

4.1 Environmental Input Parameters: Model of the Turbine and Environment

MEDUSA requires input about the following properties: *sound speed profile, sound source location, ground impedance, frequency, atmospheric absorp-*

tion, and *receiver height*. By fixing these properties, we have effectively modeled the noise source and surrounding environment. The model is constructed to describe the propagation of noise at the WTS-4 site at Medicine Bow, Wyoming (see Chapter 2).

1. *Sound speed profile*. Recall that in Section 3.4 the propagation speed is constructed as the sum of the static sound speed c_0 and the wind velocity w (see Eq. (3.2)). The static sound speed is assumed to be constant (the temperatures at the date of Willshire's 1984 measurements was not available; at the date of the 1985 experiments the temperature varied between 15°–20°), i.e. $c_0 = 343$ m/s, the sound speed in air at 20°C [14]. The form of w remains to be determined. Because the ground surrounding the WTS-4 machine is very flat, the wind can be modeled as turbulent flow over a flat plane. The well known solution (for example, see § 42 of Ref. 25) for the velocity field in this case has a logarithmic velocity profile,

$$w = K v_f \ln \left(1 + \frac{z}{z_0} \right) \quad , \tag{4.1}$$

where K is the von Karman coefficient, v_f is the friction velocity, z_0 is the friction height, and z the height above the ground. The values used here are the following: $K = 2.5$, $v_f = .64$, and $z_0 = 0.1$.

2. *Sound source character and location*. The source of the low frequency noise is the passage of the turbine blade through the turbulent wake of the support tower (see Section 2.4). Hence, the source is placed 40 m above the ground. Although we have noted that the source has dipole characteristics in the plan view (see Fig. 2.5), we have restricted our investigation to the directly downwind direction. Consequently, the directivity does not affect the field in which we are interested, and we treat the source as if it were a compact, omnidirectional source.

3. *Ground impedance*. Because waves which have undergone multiple

34

reflections are an important part of our investigation, the reflection coefficient must be specified. The reflection coefficient R_p for an air-ground interface is given by Eq. (1.5). The impedance of air Z_{air} is well known (415 in MKS units for air at 20°C [14]). The impedance of the ground is harder to obtain. We have chosen to use the empirical formula of Delany and Bazley [18]. After measuring characteristic impedance for a large number of fibrous absorbent materials, they constructed a power-law formula for the impedance. The important quantity is the ratio of the frequency f to the flow resistivity per unit thickness σ. As formulated by Chessel [19], the Delany-Bazley formula for the impedance Z is given by $Z = R + iX$, where the resistance R is

$$R/\rho_0 c_0 = 1 + 9.08(f/\sigma)^{-.75} \quad , \tag{4.2}$$

and the reactance X is

$$X/\rho_0 c_0 = 11.9(f/\sigma)^{-.73} \quad . \tag{4.3}$$

We have assumed that the flow resistivity for the ground at the WTS-4 site is $\sigma = 10^6$ in MKS units. This choice of σ agrees with experimental measurements of the ground impedance.[1]

4. *Frequency.* Although the ray paths are independent of frequency, MEDUSA requires frequency information to compute absorption and the ground reflection coefficient (see Eqs. (4.2) and (4.3)). The frequency is 8 Hz for the examples in the next section. Note that we have not accounted for the fact that the low frequency noise from the WTS-4 wind turbine is impulsive. However, since linear acoustics is assumed, the components of the pulse can be treated separately and used to reconstruct the pulse at any receiver range.

---

[1]Willshire has measured the ground impedance for frequencies above 25 Hz and found good agreement between the measurements and the Delany-Bazley model.

5. *Absorption.* We have decided to ignore air absorption in our investigation because of the very low frequencies involved. However, if it is necessary to include absorption MEDUSA can accept absorption data in tabular form or an analytic expression for absorption as a separate subroutine.

6. *Receiver height.* To compute the propagation loss, MEDUSA uses information gathered from *eigenrays.* Eigenrays are the unique rays which pass between the source and receiver. Hence the receiver height as well as its range must be specified. The microphones used in Willshire's experiments were placed almost on the ground. We used a receiver height of 0.5 m because if 0.0 m (ground level) is used it would be very difficult for MEDUSA to distinguish between an incident ray and a ray just reflected from the ground. It becomes increasingly difficult for MEDUSA to make the distinction as the receiver is placed closer to the ground. Our choice was to place the receiver near enough to the ground to study the near-ground sound field but sufficiently far above the ground to make MEDUSA's computations easier. Note that in the frequency range we are considering (2-20 Hz), the difference between 0.0 m and 0.5 m is a very small fraction of a wavelength.

To summarize, we have assumed the propagation speed is given by the scalar sum of the static sound speed c_0 and the wind velocity given by Eq. (4.1), the source is located 40 m above the ground, the ground impedance is given by Eqs. (4.2) and (4.3), and the receiver height is 0.5 m. These input parameters are used in the next section to generate examples of MEDUSA application programs. The examples are then compared with Willshire's field data in Chapter 5.

4.2 Applications of MEDUSA

After the environmental parameters described in Section 4.1 are in the input data file, MEDUSA's applications programs can be executed. The output of these programs (*ray path plots, propagation loss plots,* and *caustic plots*) provide results of our investigation. Example plots and a description of each application are described in this section. These examples are described in more detail in the next chapter; they are included here primarily for illustration.

1. *Ray paths.* Given a launch angle, MEDUSA can solve the ray equation Eq. (3.4) for the ray height as a function of range $z = z(r)$. Once the solution is obtained, MEDUSA can easily plot $z(r)$, i.e., the ray path plot. The ray path plots are probably the most widely used application of ray theory because they provide a gross description of the sound field.

Figure 4.1 shows the ray path plot for a family of rays having launch angles between $\pm 8°$ in 1° increments for the input parameters described in Section 4.1. Because of the scale of the figure (meters versus kilometers), the wedge of rays appears much larger. Note that the rays between $\pm 5°$ or $\pm 6°$ are trapped near the ground. Rays launched at greater angles do not contribute to the sound field near the ground within the first 5 km. Because the sound field near the ground is dominated by the rays launched at such small angles, the assumption in Chapter 3 that $\cos\theta \simeq 1$ is a good one.

2. *Propagation loss.* Although ray path plots provide a descriptive picture of the sound field, quantitative sound level predictions can only be made from propagation loss (PL) plots. In fact, with the aid of PL plots we will compare ray theory predictions to actual sound level data.

In qualitative terms, propagation loss is the decrease in sound level as
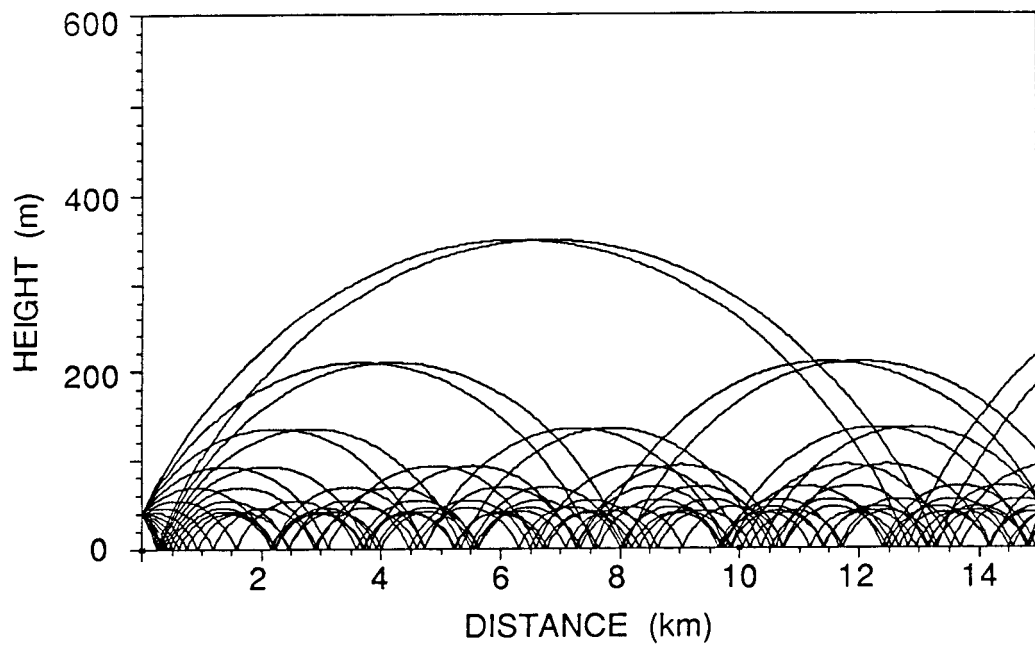
Figure 4.1 FAMILY OF RAYS HAVING LAUNCH ANGLES BETWEEN ±8°. INCREMENTS ARE 1°

one moves away from the source. The quantitative definition is

$$PL = -10 \log_{10} \left(\frac{I}{I_0} \right) \quad , \tag{4.4}$$

where I_0 is the intensity of the source and I is the intensity at the field point (a given height above the ground). The ratio I/I_0 is called the *focusing factor*. Figure 4.2 shows the PL curve for an 8 Hz component with the parameters described in Section 4.1. The solid curve is the *coherent* propagation loss, which is found by summing the received pressure signals, including phase, from each eigenray and using the sum to obtain the intensity.[2] The dotted curve is a reference and represents the loss due to ordinary spherical spreading in a homogeneous atmosphere.

As previously noted, the central theme of this thesis is the application of ray theory to study the propagation of low frequency turbine noise. The success of the application can be only judged by comparing the ray theory predictions to actual sound field data. The PL curve provides the basis for a direct comparison between the data and the ray theory predictions. In Chapter 5 we will discuss the comparison in more detail. The importance of caustics is described in the remainder of this chapter.

3. *Caustics.* In the investigation of sound propagation from the WTS-4 wind turbine we have assumed as a first approximation that caustics need not be accounted for when calculating the PL curve. Figure 4.3 shows the location of

---

[2]Although it is not included in Fig. 4.2, an *incoherent* propagation loss can be calculated by MEDUSA. In the calculation, the phase of each contribution to the field intensity is ignored, and a $1/\sqrt{2}$ is substituted to account for losses attributable to phase differences. We calculated the incoherent PL for this example. It has the same general shape as the coherent PL curve, but because of the factor $1/\sqrt{2}$ the propagation loss is greater. Consequently, the incoherent PL curve is closer to the spherical spreading curve. Incoherent PL is used in cases where phase differences cause complications in the PL curve. In our investigation it was not necessary to calculate incoherent propagation loss.
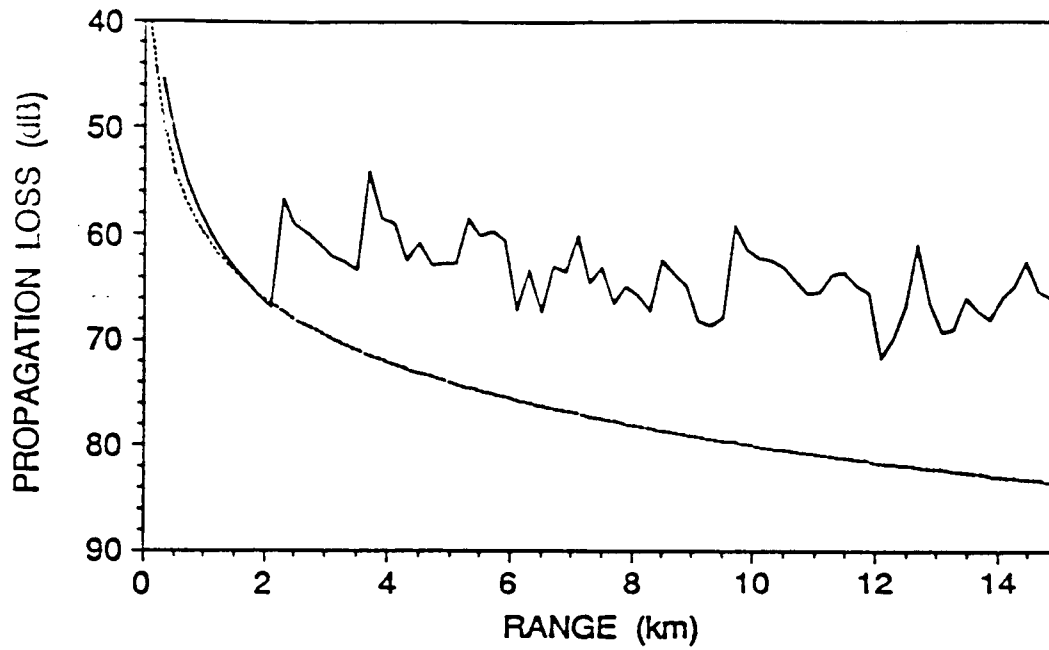
Figure 4.2 Propagation loss for ranges out to 15 km.
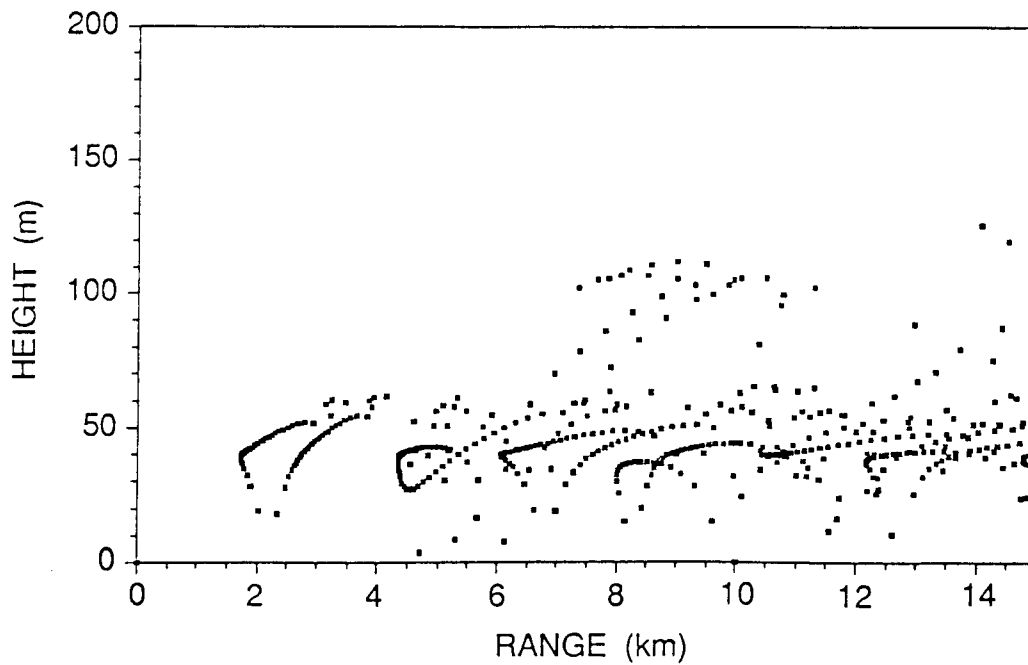
Figure 4.3 Location of caustics.

40

caustics for the sound field depicted in Fig. 4.1. Note that few caustics occur near the ground. Although our neglect of caustics when we compute intensity cannot be defended quantitatively, it is clear that few caustics occur near the ground, where our field points are located. We therefore assume that simple ray theory is valid for the calculations in which we are interested.

After careful selection of input parameters (Section 4.1) which model the WTS-4 machine and its environs, we have seen that the example applications (Section 4.2) of MEDUSA provide theoretical predictions for comparison with Willshire's experimental results. In the next chapter we examine these applications in more detail.

CHAPTER 5

APPLICATIONS TO WILLSHIRE'S SEPTEMBER 1984 EXPERIMENTS

In this chapter we look more closely at the applications of ray theory described in Chapter 4 and the data with which the theory is compared. In particular, the sound level data gathered by W. L. Willshire at the WTS-4 wind turbine at Medicine Bow, Wyoming, in September 1984 is compared to the PL curve predicted using MEDUSA. A detailed description of Willshire's data is given in the first section.

5.1 Experimental Data

During September 1984 W. L. Willshire made detailed measurements of low frequency (2-20 Hz) noise of the WTS-4 wind turbine located at Medicine Bow, Wyoming.[1] In 1985 Willshire gave both an oral report [24] and a written report [5] that describe the results.

Data were collected downwind of the turbine during a 4 hour period of a single day. Willshire sampled the sound field at nine different recording sites

---

[1]Mid-frequency (63 Hz, 250 Hz, and 1000 Hz) data are included in Willshire's results, but the main emphasis of Willshire's 1985 report is on the low frequency noise. We briefly discuss the mid-frequency results in Appendix E.
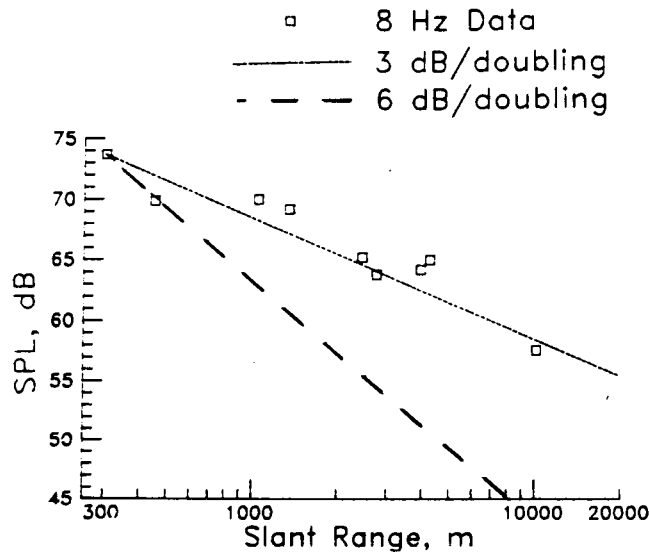
Figure 5.1 Sound level measurements at the WTS-4 site (from Ref. 5).

located 0.3 km to 10 km from the turbine. Each measurement was made separately. During the course of the experiment, the wind speed range was 12-15 m/s. Sound levels in the 2-20 Hz frequency range were measured. The sound levels at 6, 8, and 11 Hz were singled out for presentation in Willshire's report because of their good signal to noise ratio and "low source variablility." A reproduction of Willshire's plot of the 8 Hz data is shown in Fig. 5.1 (from Ref. 5).

In Fig. 5.1, the sound pressure level (in decibels) is plotted versus the logarithm of the slant range. Slant range, which is the line-of-sight distance from the source to the receiver, was used because the source is elevated (recall that the source of the thumping noise is assumed to be 40 m above the ground). The lower (dashed) line is the curve for a signal subject only to spherical spreading, that is, 6 dB loss of signal strength per doubling of distance. The upper line is the

curve for a cylindrically spreading signal. Note that the two data points nearest the source fall on the spherical spreading curve, while the downrange data points closely follow the cylindrical spreading curve. In other words, the pattern implies spherical spreading near the source and cylindrical spreading downrange. This pattern occurs in all of Willshire's low frequency data.

At first glance, the high sound levels for the downrange data are somewhat unexpected. Since we are investigating low frequency components, atmospheric absorption is considered negligible. Hence, one might expect the sound levels to closely follow the spherical spreading curve. However, this expectation proves to be mistaken, as will be seen when the PL curve based on ray theory is examined. In Section 5.3, we compare propagation loss predictions based on ray theory with the data described in this section. Before proceeding, we will examine the ray plot of Fig. 4.1 more closely.

5.2 Ray Paths near the Source (0-2 km)

Shown in Fig. 5.2 is a closer view of the ray paths plotted in Fig. 4.1. The sound field is shown up to a height of 200 m and out to a range of 5 km. Notice that near the source only single ray arrivals are recorded. Since atmospheric absorption is considered negligible and the rays have not yet hit the ground more than once, the only contribution to the diminution of the sound level is spherical spreading of the sound (modified only slightly by refraction). At some distance downrange (≈ 2 km), the onset of a confluence of rays can be seen. Thereafter the sound field on the ground is characterized by multiple ray arrivals. The arrival of additional rays should cause a significant increase in the sound level.
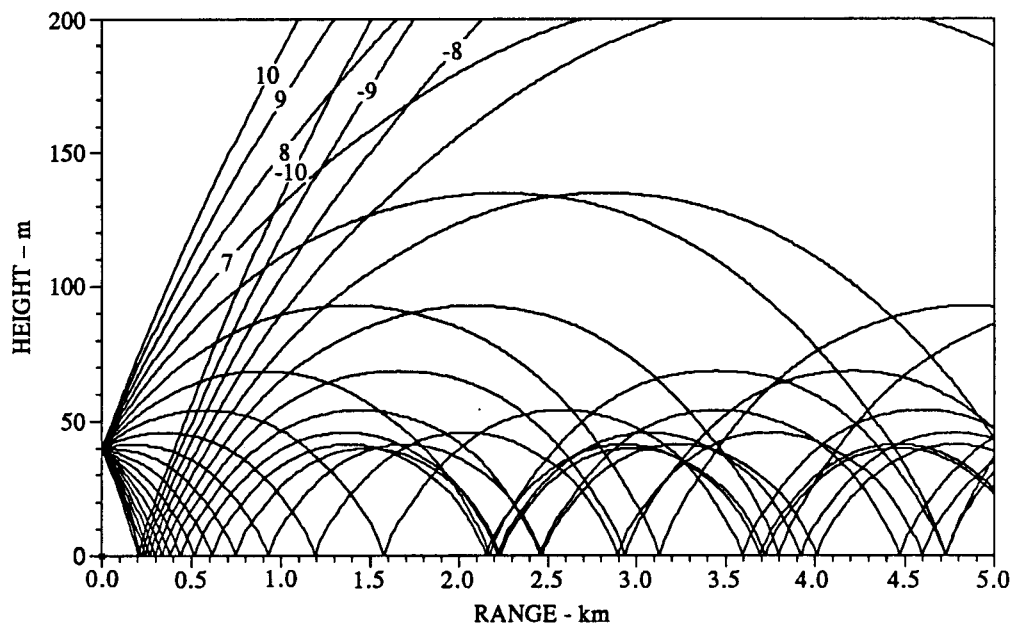
Figure 5.2 FAMILY OF RAYS HAVING LAUNCH ANGLES BETWEEN ±10°. LAUNCH ANGLE INCREMENT IS 1°.

5.3 Propagation loss

We now turn to the propagation prediction based on ray theory. In Figs. 5.3-5.5 the ray theory PL curve (see Fig. 4.2) has been reproduced with Willshire's 6, 8, and 11 Hz data points, respectively. Recall that the upper curve is the propagation loss for the windy atmosphere, while the lower curve represents spherical spreading. We note here that the spherical spreading curve represents the diminution of sound due solely to increasing *slant range R*, i.e., $PL \propto -20 \log 1/R$, where the slant range R is the line-of-sight distance from the source to the receiver. The loss is computed with slant range; however, it is plotted versus range along the ground r.

Willshire's data are added to the PL plots in the following manner. First, we assume spherical spreading near the source. Consequently, the 300 m data point is placed on the spherical spreading curve in the PL plot. The remaining data points are plotted relative to spherical spreading from 300 m. That is, the loss due to spherical spreading from 300 m is subtracted from the actual measurement. The result is the relative level. The relative level is then added to the MEDUSA calculated spherical spreading curve. Clearly, good general agreement is obtained between the experimental data and the ray theory PL curve.

The sharp jumps of the ray theory curve are explained as follows. As an example, consider Figs. 5.3 and 5.4. Inspection shows that the jumps in the PL curve are associated with the onset of multiple ray arrivals at the receiver. In fact, MEDUSA computes an eigenray data summary which tells us exactly where the jumps occur. For example, out to the range of the first jump, just beyond 2.1 km, only two eigenrays are recorded at each receiver range: one direct eigenray and one eigenray which reflects from the ground just in front of the receiver. Between

46
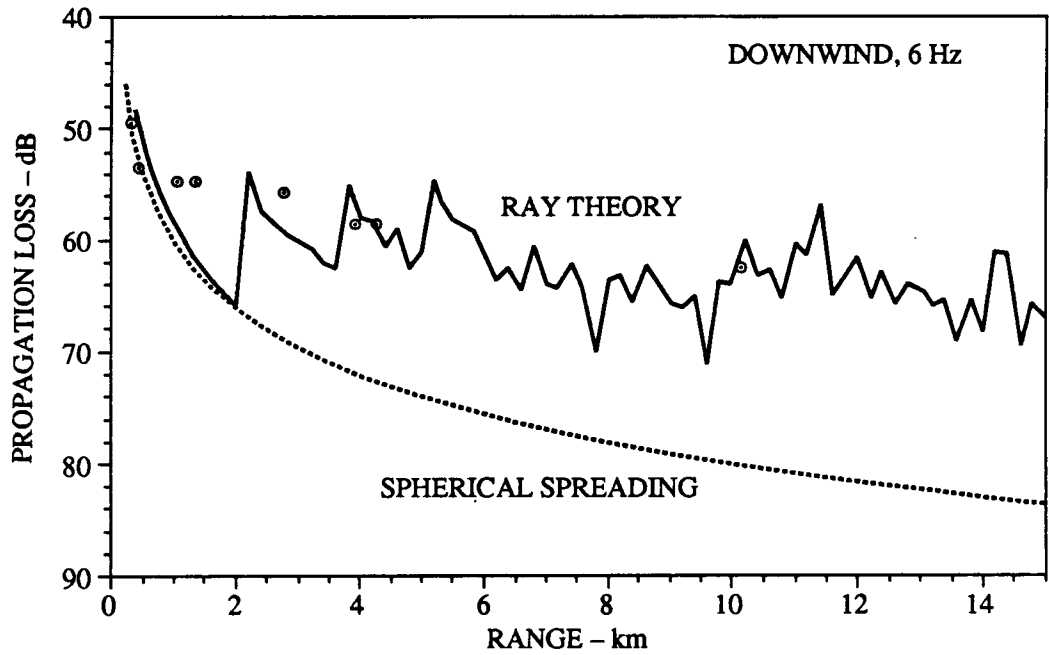
Figure 5.3 Propagation loss at 6 Hz with Willshire's data added.
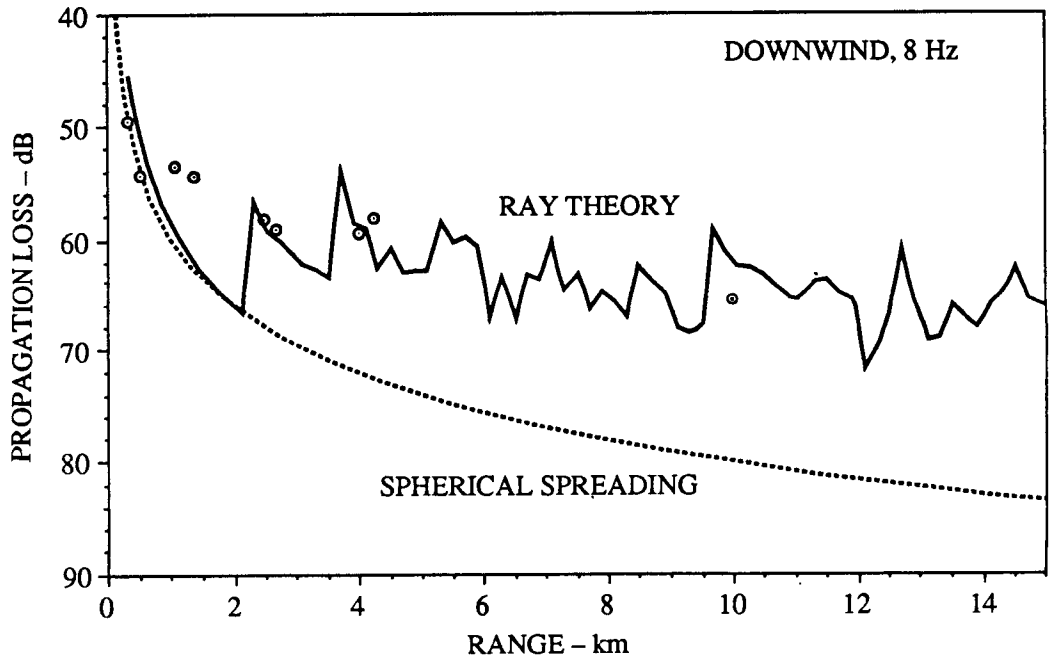
Figure 5.4 Propagation loss at 8 Hz with Willshire's data added.

47
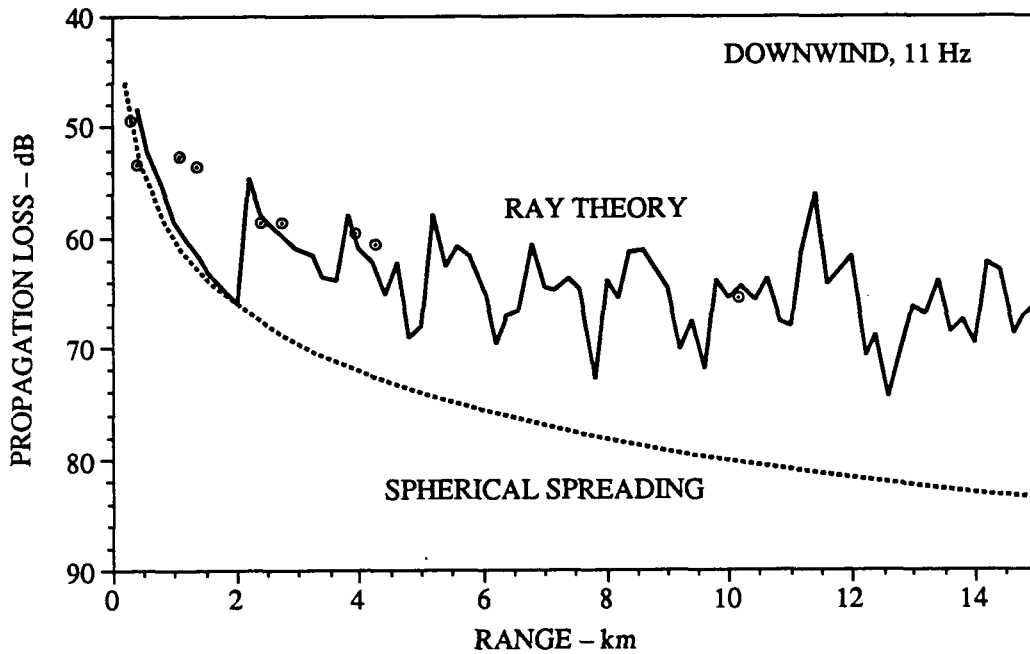
Figure 5.5 PROPAGATION LOSS AT 11 Hz WITH WILLSHIRE'S DATA ADDED.

2.1 and 2.3 km four additional eigenrays are found making a total of six eigenrays at the 2.3 km range. Because we have instructed MEDUSA to search for eigenrays in 0.2 km steps, we do not know exactly where the additional rays arrive—it is known only that the additional rays arrive somewhere between 2.1 km and 2.3 km. Nevertheless, there is a sharp jump in the PL curve at 2.3 km. After 2.3 km, the number of eigenrays remains constant until about 3.7 km, where another jump occurs. Because the number of eigenrays between 2.3 km and 3.7 km is constant, the only contribution to propagation loss is travel distance. Therefore, the PL curve between these two points drops off with a spherically spreading slope. Although jumps can be seen at longer distances, the PL curve becomes more complicated. Jumps and drops occur in a less regular manner.

We have noted that the ray theory PL curve lies considerably above the spherical spreading curve. In fact, we know from Willshire's data that the

48

spreading is cylindrical. The observed and (ray theory) predicted propagation loss behavior is consistent with our understanding of sound in a channel [26]. A channel is formed because downwind sound rays that propagate close to and almost parallel to the ground are trapped near the ground. Furthermore, after reflection at the ground, they always return to the ground (see Fig. 5.2). Evidently, Willshire's measurements reveal a sound channel downwind of the WTS-4 machine.

Although ray theory is successfully applied to the problem of propagation of low freqency noise from the WTS-4 wind turbine, certain minor discrepancies may be noted. Again consider Fig. 5.3. First, careful inspection of the figure shows that the spherical spreading curve first falls slightly below the ray theory predicted curve and then approaches it. Two opposing effects are at work. First, very near the source, the difference exists because MEDUSA locates eigenray pairs. Therefore the ray theory curve should be above (on the order of 6 dB) the spherical spreading curve near the source. In the region between 500-1500 m, however, the ray theory curve approaches and even falls below the spherical spreading curve. Recall from Section 5.2 that we assume spherical spreading is dominant near the source. Since the rays follow curved paths rather than straight lines, one might expect deviation from $1/r$ losses. In fact, because of strong refraction of the rays toward the ground, the ray tube area (see Appendix D) increases more rapidly than it would in a homogeneous medium. The propagation loss is therefore greater than that of spherical spreading. However, the effects just described are minor compared with the changes associated with the onset of multiple ray arrivals at about 2.0 km.

Second, the two data points at ranges near 1000 m fall considerably above the spherical spreading curve. Their position may indicate that the channel

region begins slightly nearer the source than predicted by ray theory. However, the location of each jump is expected to vary with temporal changes in the sound speed profile (both short term fluctuations and longer term variations). Data taken over a relatively long time (recall that Willshire's measurements were made separately over a 4 hour period) would therefore be expected to define an average curve, not one based on a very specific sound speed profile. (In Chapter 6 we will compare our ray theory predictions with data taken over a very short time interval.) Consequently, because of the problems associated with collecting data in a windy atmosphere, the data should not be expected to exactly fit the ray theory curve. Another possibility is that the levels at 1000 m might be the result of diffraction from a caustic (see Appendix D). However, from Fig. 4.3 we see that the nearest caustics are 1000 m away from the data points. It is unlikely that caustics at such a distance would have any effect.

By directly comparing the ray theory PL curve with the data, we can conclude that the basic features of the sound field measured by Willshire— spherical spreading near the source and cylindrical spreading downrange—are to be expected. In fact, the wind gradients near the ground downwind of the WTS-4 turbine create an atmospheric sound channel in the downwind direction. Sound channels are a well known phenomenon of underwater acoustics and are characterized by cylindrical spreading [26]. That the downwind atmospheric sound channel exists is amply supported by Willshire's data. The data points which fall on the spherical spreading curve near the source simply show that the sound channel has yet to be formed.

In conclusion, we see that the exact shape of the PL curve for a particular time is not available from ray theory. Nevertheless, the general shape of the PL curve—spherical spreading near the source and cylindrical spreading

50

downrange—accurately reflects the acoustics of downwind low frequency sound from the WTS-4 wind turbine. In the next chapter we compare ray theory predictions with data, both upwind and downwind, taken in Willshire's more elaborate experiments carried out in May-June 1985.

CHAPTER 6

APPLICATIONS TO EXPERIMENTS CONDUCTED DURING
MAY-JUNE 1985

Because of interest generated by Willshire's first experiment (September 1984), more experiments were conducted during the following spring, in May-June 1985. Both upwind and downwind measurements were made, as well as a few measurements at other angles of azimuth. We are concerned here with just the upwind and downwind data. Although we have not analyzed all of the new data, an analysis of a representative portion, which we feel illustrates the main observations, has been completed. The results of the analysis are described in this chapter.

The data from the 1985 experiment are sound pressure levels for frequencies between 1 and 20 Hz. The levels were obtained with special B&K low frequency microphones and recorded as digitized data (100 pps sampling rate) using a 4096-point fast Fourier transform (FFT). Each *data run* consists of blocks of data for the frequency components from which which we computed average SPLs. Only levels with a 3 dB signal-to-noise ratio were included in our investigation. Recall that we have assumed that the sound is propagating over flat ground.[1]

---

[1]We note here that there is some concern about the location of the 10,000 m microphone. While the ground is flat out to 6-7 km, thereafter the ground dips some 30 ft and then rises in stages to about 10 ft above 'level' ground. The microphone was positioned on the rise.

Atmospheric conditions during the 1985 experiments were comparable to those of the 1984 experiments. The temperature range was typically within a few degrees of $20°C$. Wind speed varied from about 9 m/s to 24 m/s. The wind direction varied from the directly downwind direction between $+32°$ and $-47°$. Table 6.1 contains the ranges of measurements for the 1984 and 1985 experiments.

Table 6.1 RANGES FOR THE 1984 AND 1985 EXPERIMENTS.

Range along the ground (m)	
September 1984	May-June 1985
292	350
444	608
1048	838
1353	1749
2447	2006
2752	2242
3952	4851
4257	10,000
10147	20,000

Before proceeding we point out an important difference between the two experiments. Recall that the fall 1984 measurements were made with a single microphone over a 4 hour period, i.e., Willshire made consecutive, not simultaneous, measurements as the distance from the turbine was changed. Consequently, the data give only an average picture of the downwind sound field. In contrast, the May-June 1985 measurements were made simultaneously; each measurement site had its own microphone. In the second experiment each *data run* lasted only long enough—a few minutes—to obtain a time average of the sound levels. In the second experiment, therefore, an instantaneous 'snapshot' of the sound field was obtained.

6.1 Modification of the Theory To Include Upwind Propagation

A short discussion of how the data is compared to ray theory is now given. The downwind data is compared to the theory in exactly the same manner as described in Chapter 5. However, to discuss the upwind data we must modify our expression for the propagation speed. Recall in Section 3.4 that we constructed the propagation speed by adding the component of the wind velocity in the direction of propagation to the static sound speed. For upwind propagation, we subtract the wind velocity from the static sound speed, i.e.,

$$a_{upwind} = c_0 - w \cos \theta \quad .$$

(6.1)

Again, we make the approximation $\cos \theta \simeq 1$. As we shall see, the propagation speed profile in this case leads to the formation of a shadow zone. Since ray theory cannot be used to accurately predict sound levels in a shadow zone (see Appendix D), one should expect considerable discrepancy between predictions and data for upwind propagation.

6.2 Downwind Sound Levels (dB)

As seen in Chapter 5, our ray theory predictions give a good account of the data recorded in the first experiment, in particular, spherical spreading near the noise source and cylindrical spreading downrange. Do the downwind propagation results of the second experiment provide the same good correlation between data and prediction?

Figures 6.1-6.4 show the measured SPLs at 10 Hz versus the logarithm of the range for four data runs. Furthermore, a cylindrical spreading, or 3 dB per doubling of distance, curve (dash-dot-dash curve) and a spherical spreading,

54
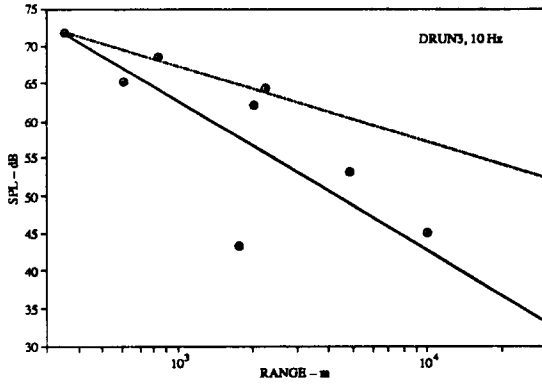
Figure 6.1 DOWNWIND EXPERIMENT NO. 3, 10 Hz.
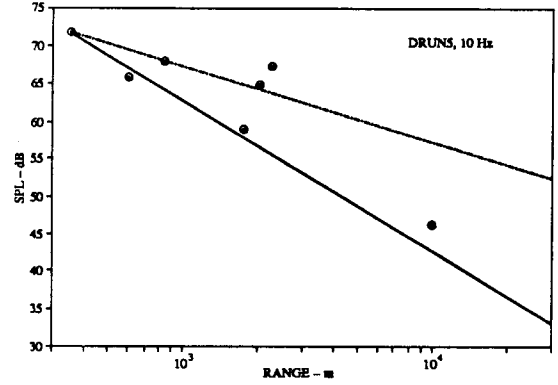
Figure 6.2 DOWNWIND EXPERIMENT NO. 5, 10 Hz.
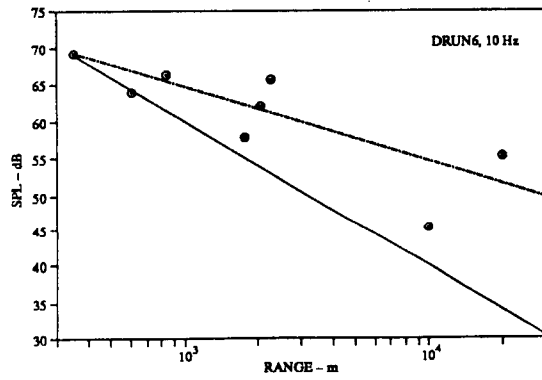
Figure 6.3 DOWNWIND EXPERIMENT NO. 6, 10 Hz.
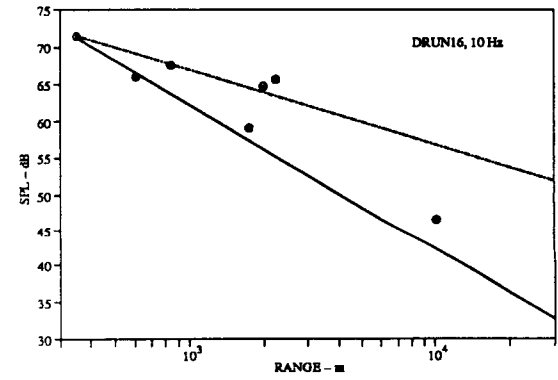
Figure 6.4 DOWNWIND EXPERIMENT No. 16, 10 Hz.

Table 6.2 LIST OF WIND CONDITIONS FOR DOWNWIND EXPERIMENTS.

Figure	Data run	Wind speed (m/s)
6.1	DRUN3	15
6.2	DRUN5	14
6.3	DRUN6	16
6.4	DRUN16	18

or 6 dB per doubling of distance, curve (solid curve) are shown for comparison. The data are plotted in this manner in order to retain the same format used by Willshire (see Section 5.1). Table 6.2 lists four data runs and the wind speed at the hub at the time of the measurements.

We comment on the general features of the data in Figs. 6.1-6.4. In all of the figures, the data points within the first 1000 m exhibit spherical spreading. The next three data points (near 2000 m) are near the cylindrical spreading curve which indicates the formation of the sound channel. The 10,000 m data points fall much nearer the spherical spreading curve. Finally, the 20,000 m data point from run 6 falls near the cylindrical spreading curve (the measurement at 20,000 m was difficult to obtain, hence the sparsity of data at that range).

While the data from Willshire's first experiment consistently exhibit spherical spreading near the source and cylindrical spreading downrange, no clear trends exist for the new data. In fact, the data in Figs. 6.1-6.4 are scattered between the cylindrical and spherical spreading curves.The fluctuation in the sound levels between spherical and cylindrical spreading seems puzzling.[2]

---

[2]The location of the 10,000 m microphone was atypical in that the ground was undulating, not flat (see footnote p. 52). If, because of the undulations, the microphone was shielded from some of the reflected rays, an unusually low sound pressure level would have been recorded.

6.3 Least Squares Fit of the Downwind Data

Perhaps because of the puzzling scatter of the data, Hubbard, Shepherd, and Willshire [27], in a brief presentation of the measurements for seven of the downwind data runs, chose to present a least squares fit curve for each run. The seven curves completely cover the region between the spherical and cylindrical spreading curves, except for one run, which lies about 3 dB above the cylindrical spreading curves. In this section we present the least squares fit for the data runs shown in Figs. 6.1-6.4.

Figures 6.1-6.4 are reproduced in Figs. 6.5-6.8, with the exception that the individual data points for each run are replaced by a least squares fit (dotted curve) for that run. The fit was made by assuming that the sound pressures diminish with range according to a power law, i.e.,

$$SPL = m \log (\text{range}) + b \quad , \tag{6.2}$$

where SPL is in dB, b is the projected source sound level, and m is the slope of the curve. Both b and m are determined by the least squares algorithm.

The advantage of using the least squares fit to present the data is that the wide variation of individual data evident in Figs. 6.1-6.4 is masked. We might expect the smoothing process to obscure or hide important factors. In any case, the process clearly reveals that in all four data runs the average propagation loss falls between the cylindrical and spherical spreading curves. The spread is about the same as that found by Hubbard et al. [27]. For example, the curve for run 3 implies a near-spherical spreading of the sound while the curve for run 6 seems to confirm cylindrical spreading. One concludes that while the average curves do 'organize the data,' the new presentation still does not allow us to explain why the data behave as they do.
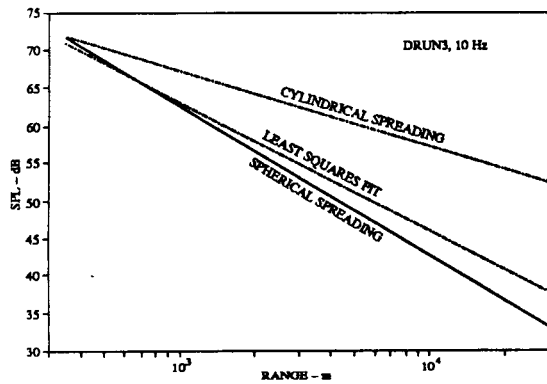
Figure 6.5 LEAST SQUARES FIT FOR DATA FROM EXPERIMENT No. 3, 10 Hz.
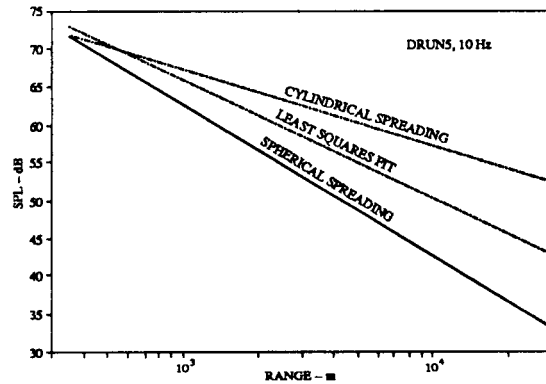
Figure 6.6 LEAST SQUARES FIT FOR DATA FROM EXPERIMENT No. 5, 10 Hz.
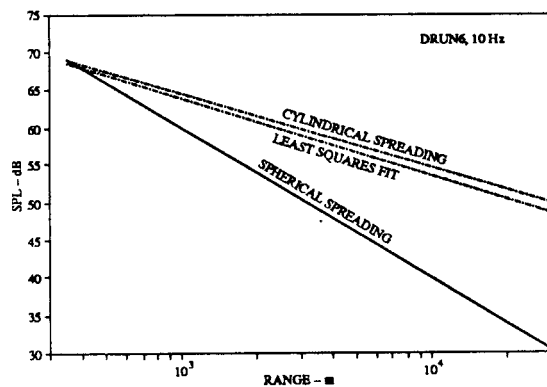
Figure 6.7 LEAST SQUARES FIT FOR DATA FROM EXPERIMENT No. 6, 10 Hz.
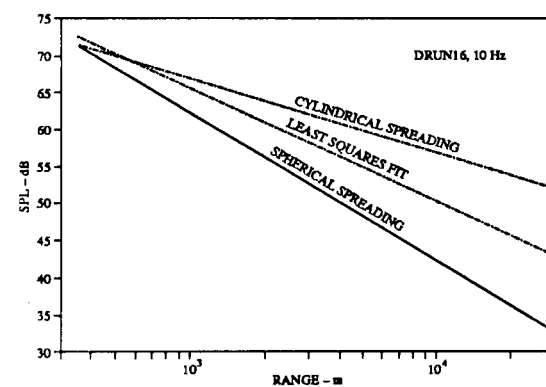
Figure 6.8 LEAST SQUARES FIT FOR DATA FROM EXPERIMENT No. 16, 10 Hz.

58

6.4 Comparison with Ray Theory Predictions

It appears, superficially at least, that the data from the second experiment does not support the conclusions based on analysis of the data from the first experiment. However, the physical argument that a sound channel forms near the ground because of strong gradients in the wind velocity still has strong appeal. It is difficult to see why a sound channel would be any less likely on a short term basis than on a long term basis.

Of particular interest are the midrange (near 2000 m) data points. In Chapter 5 we saw that near 2000 m the propagation loss curve calculated by MEDUSA has a sharp jump which indicates a confluence of rays. A possible explanation of the jumps in the data near 2000 m in the second experiment (see Figs. 6.1-6.4) is that it is due to the confluence. In Figs. 6.9-6.12 we have plotted the data from the May-June 1985 experiments with the PL curve as produced by MEDUSA. It is seen that the predicted jump does indeed correlate very well with the behavior of the data in that region. In fact, except for data run 3, not only the position but also the magnitude of the observed jump is correctly predicted.

Agreement between prediction and measurement is not as good at the far downrange points, particularly at 10 km. However, as has already been pointed out, the environment at the 10 km measurement site was somewhat atypical. Moreover, the 20 km data point in run 6 does confirm the MEDUSA prediction.

Except for scatter in some of the far downrange data points, the May-June 1985 experiments also indicate a downwind sound channel. The PL curve again provides a good prediction of the observed field. In fact, the confirmation is better in the second experiment because data were taken near 2000 m, the range at which the first jump is predicted to occur.
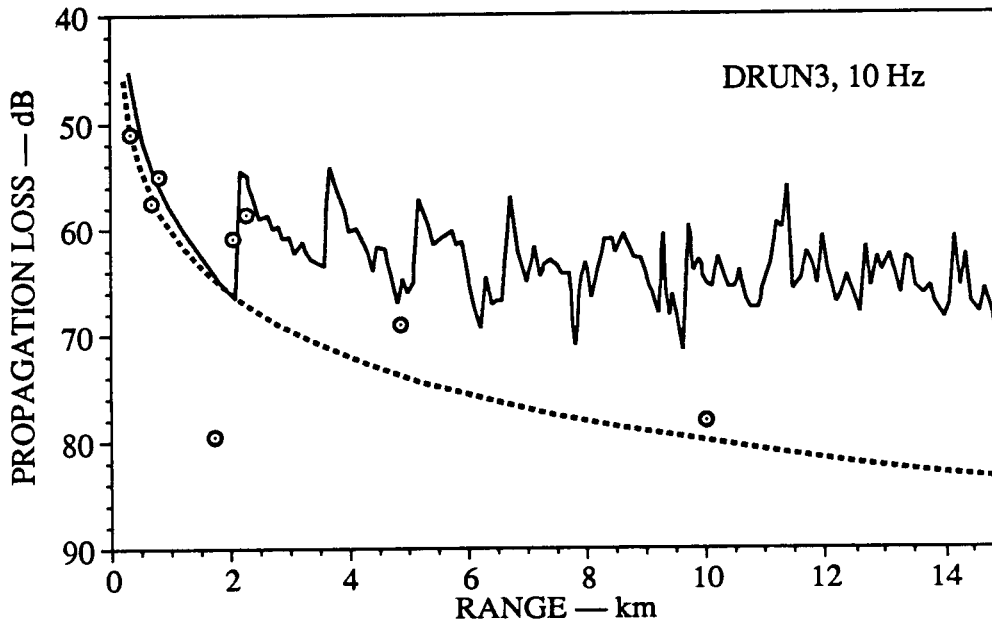
Figure 6.9 PROPAGATION LOSS WITH DATA FROM EXPERIMENT No. 3, 10 Hz.
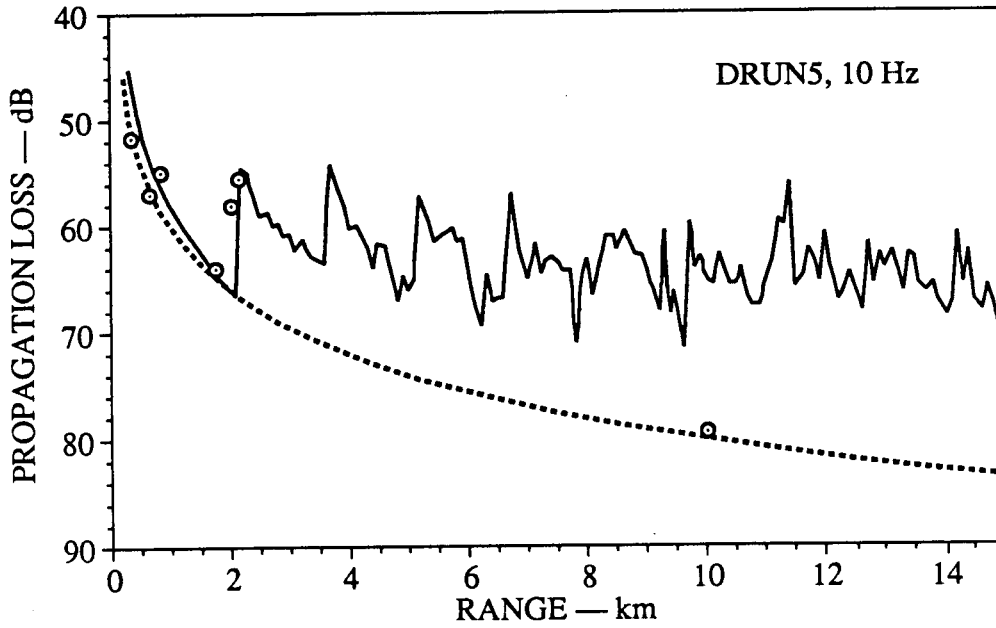
Figure 6.10 PROPAGATION LOSS WITH DATA FROM EXPERIMENT No. 5, 10 Hz.
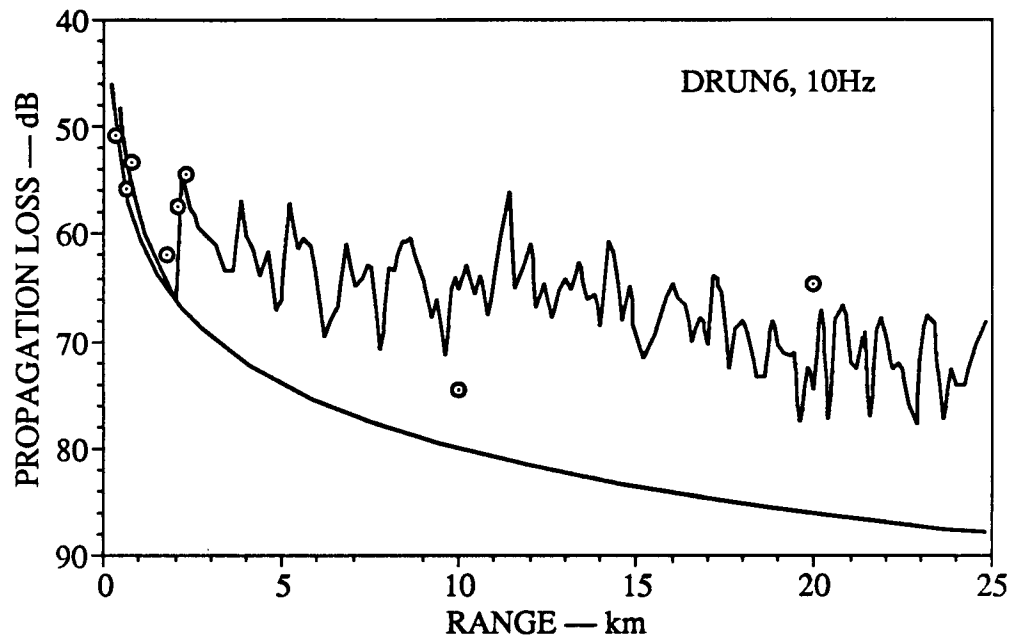
Figure 6.11 PROPAGATION LOSS WITH DATA FROM EXPERIMENT No. 6, 10 Hz.
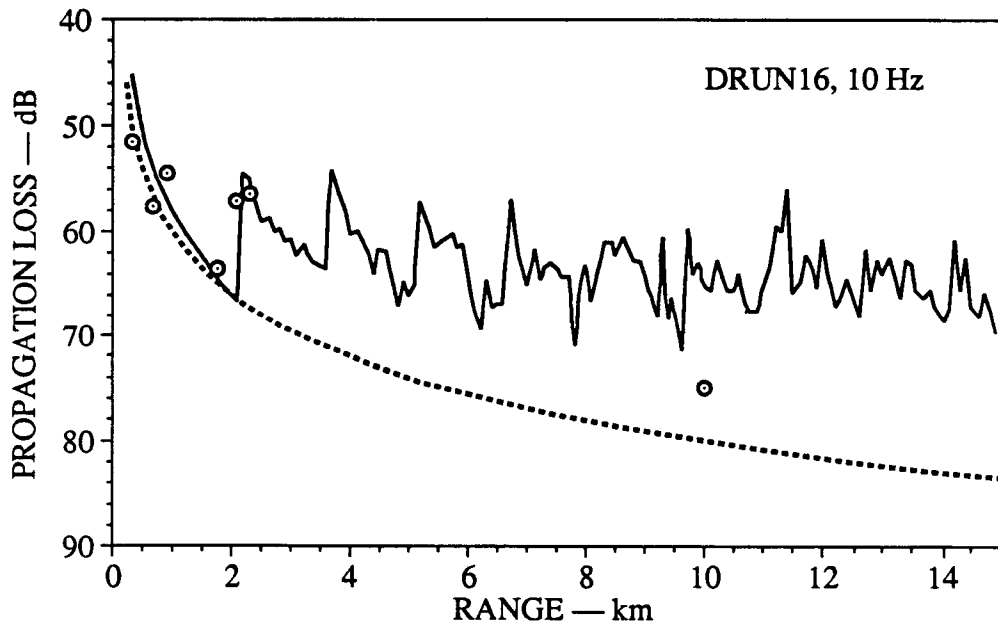
Figure 6.12 PROPAGATION LOSS WITH DATA FROM EXPERIMENT No. 16, 10 Hz.

Table 6.3 LIST OF WIND CONDITIONS FOR EXPERIMENTS SHOWN IN FIG. 1.

Figure	Data run	Wind speed (m/s)
1	URUN29	12
2	URUN30	15
3	URUN8	11
4	URUN18	15

6.5 Upwind Data

The May-June 1985 experiments included measurements of the upwind sound levels from the WTS-4 wind turbine. Figures 6.13-6.16 show the upwind SPLs at 10 Hz versus the logarithm of the slant range for four of the upwind data runs. Conditions for these experiments are shown in Table 6.3. For comparison, curves for cylindrical spreading, or 3 dB per doubling of distance (upper curve), and spherical spreading, or 6 dB per doubling of distance (lower curve), are also shown. Note that in each figure the left end of the abscissa is 200 m, not 100 m. Table 6.4 is a list of the ranges at which data were collected. For the experiments shown in Figs. 6.13, 6.14, and 6.16, the measurement nearest the WTS-4 machine was made at 201 m. This data point is used as the anchor from which the spherical and cylindrical spreading curves are drawn. For Fig. 6.15 the nearest measurement was at 400 m; consequently, the spherical and cylindrical spreading curves begin there. The group of data points from near 650 m to just under 1150 m are clustered around the spherical spreading curve. The last three data points (the region between 2450 m to 2950 m) are generally below spherical spreading. In the data runs shown here no 3660 m measurement was recorded. In summary the data in Figs. 6.13-6.16 show that in the region of 200-1150 m the SPLs closely follow the spherical spreading curve. At longer ranges, however, the levels are somewhat lower.

62
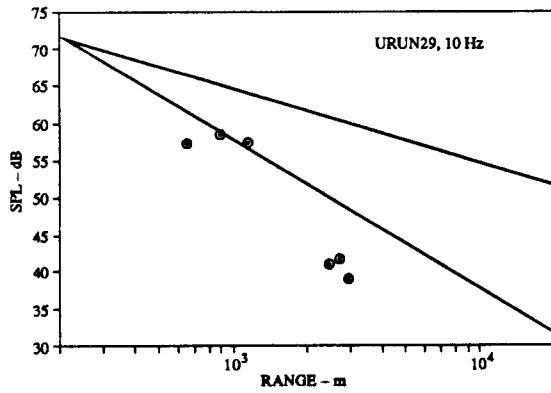
Figure 6.13 UPWIND EXPERIMENT No. 29, 10 Hz.
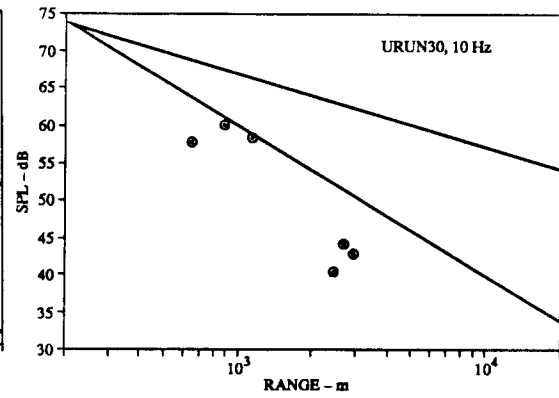
Figure 6.14 UPWIND EXPERIMENT No. 30, 10 Hz.
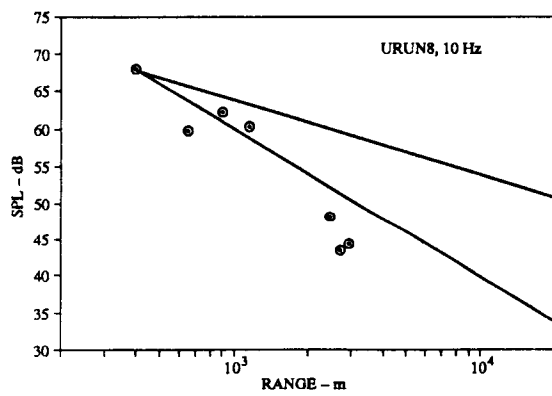
Figure 6.15 UPWIND EXPERIMENT No. 8, 10 Hz.
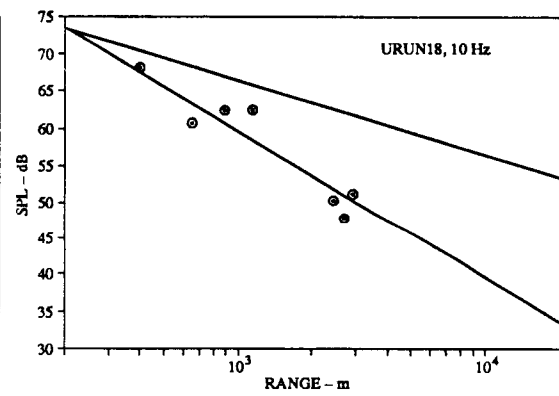
Figure 6.16 UPWIND EXPERIMENT No. 18, 10 Hz.

Table 6.4 RANGES 1985 UPWIND EXPERIMENTS.

Upwind Ranges, m
201
400
650
888
1147
2437
2684
2925
3660

How do ray theory predictions compare with the data? Because the wind 'opposes' the propagation of sound upwind of the WTS-4 machine, a negative sound speed gradient is formed. Consequently, we expect the formation of a shadow zone [10] in which the SPLs are much lower (infinitely lower if no sound leaks into the shadow zone by diffraction), than the values given by spherical spreading. In Figs. 6.13, 6.14, and 6.15 the departure from spherical spreading beyond about 1000 m is evident, and it would be tempting to conclude that ray theory is confirmed.

However, quantitative calculations show otherwise. Consider the ray trace diagram for a typical upwind profile shown in Fig. 6.17. The diagram shows that the shadow zone should begin at a range less than 300 m. More detailed computations for the upwind data runs show that the shadow zone is predicted to begin at about 180 m from the source. The upwind PL curve shown in Fig. 6.18 demonstrates the dramatic drop in the sound levels associated with the shadow zone. It is clear from the data, however, that sound is present in the upwind region beyond the boundary of the shadow zone.

64
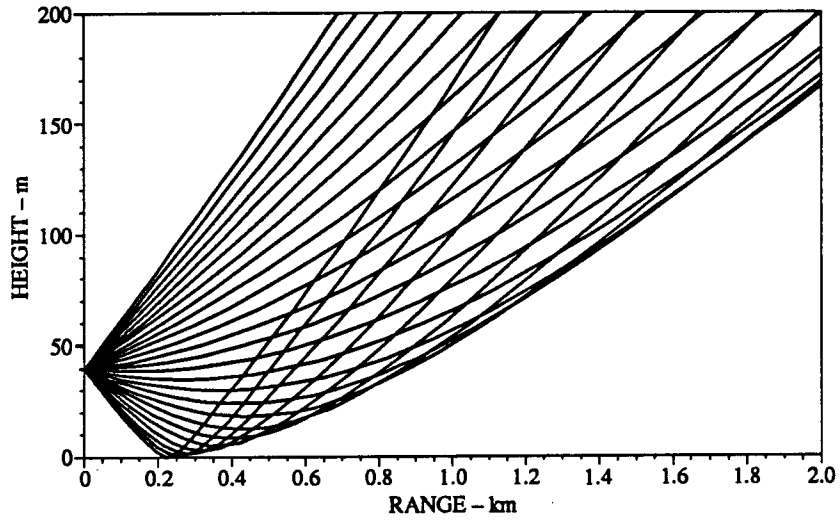
Figure 6.17 Fan of upwind rays showing the formation of a shadow zone.
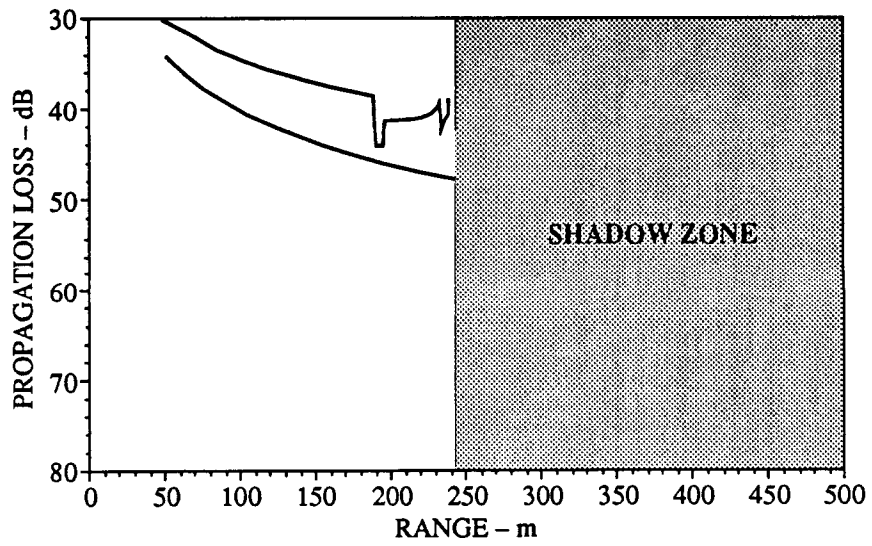
Figure 6.18 Propagation loss (8 Hz) in the upwind direction with spherical spreading curve (lower curve).

On the other hand, some reduction in SPL in addition to that due to spherical spreading is apparent. For example, if we compare the average of the four upwind SPLs runs at about 2.8 km with the average of the four downwind SPLs (interpolated at a range of 2.8 km), we see the downwind SPLs are about 59 dB whereas the upwind SPLs are about 45 dB, i.e., the SPL of the upwind sound is much less than that of the downwind sound at a comparable range. Since the microphone nearest the source was located at a range of 201 m, i.e., beyond the predicted end of the insonified region it is not possible to judge whether any significant drop associated with the shadow zone occurred. Nevertheless, one concludes that while the sharp shadow zone predicted by using ray theory does not occur, the data confirm the general expectation (based on ray theory) that the SPL should be much reduced upwind.

It is, in fact, well known that the application of ray theory in a shadow zone, because of its association with a caustic surface (see Fig. 6.19 and Appendix D), does not yield accurate sound level predictions, particularly at very low frequencies. Piercy et al. state that at low frequencies the shadow zone is poorly formed and that the sound levels in the shadow zone are generally 10-20 dB higher than the levels at high frequencies (above 400 Hz) [4]. The readiness with which the low frequency sound penetrates the shadow zone is confirmed by Willshire's measurements.

For the record several features of the PL curve given by MEDUSA for the upwind case, Fig. 6.18, are interesting. First, because refraction effects near the ground cause the ray tube area to be smaller than it would be for a homogeneous medium, and because MEDUSA locates eigenray pairs, the upwind PL curve is increasingly higher than the spherical spreading curve from 50 m to near 180 m. Second, the seemingly erratic behavior of the PL curve beyond 180 m has a

66
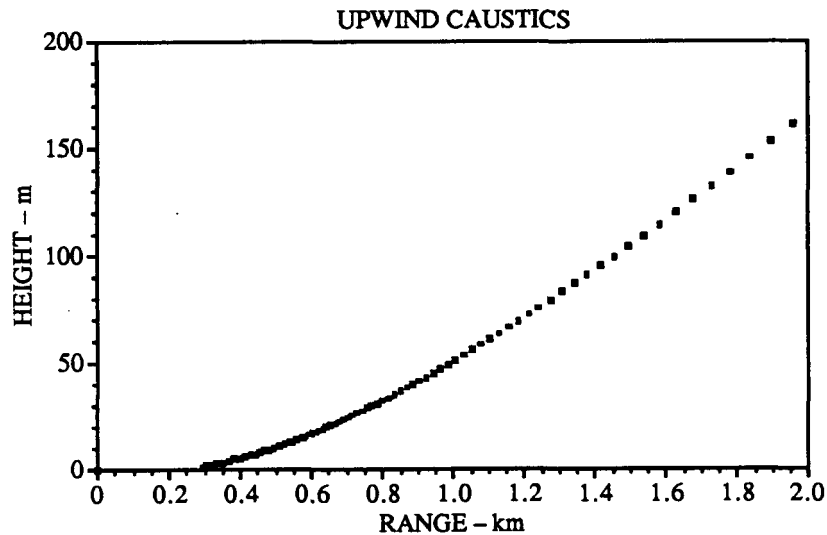
Figure 6.19 FORMATION OF CAUSTICS ALONG A SHADOW ZONE.

physical explanation. In this region MEDUSA is still locating eigenray pairs; however, because the second ray of the pair has passed through a caustic, it has suffered a $\pi/2$ phase shift. The combination of the two rays in quadrature therefore produces a drop in SPL. Thereafter, the curve rises as the observation point nears the pairs; however, a $\pi/2$ phase shift is introduced because the second ray of the pair has passed through a caustic. Thereafter, the curve rises as it nears the caustic; however, before the caustic is reached, a second drop occurs because MEDUSA can locate only one eigenray (refraction has caused the other to deflect away before ever reaching the observation point). Finally, as the observation point gets very close to the caustic, the precipitous drop in ray tube area causes the *PL* curve to rise very sharply. Not shown because of scale is the drop to infinite propagation loss, which marks the beginning of the shadow zone.

CHAPTER 7

SUMMARY AND CONCLUSIONS

In this chapter we provide a brief summary of this thesis and the conclusions that are drawn from our investigation. Suggestions for future work are discussed in Section 7.4.

7.1 Downwind Sound Field

During the fall of 1984, W. L. Willshire made measurements of the low frequency (1-20 Hz) downwind sound field of the WTS-4 wind turbine at Medicine Bow, Wyoming. Although the measurements were simple, they revealed a distinct propagation loss pattern—spherical spreading near the source and cylindrical spreading downrange. Separate investigations based on ground wave theory, normal mode theory, and the parabolic approximation were undertaken in which the objective was to provide a theoretical framework for the data.

In this thesis we attempt to use simple ray theory to explain Willshire's data. General ray theory for a moving medium is developed and the ray path equation Eq. (3.12) is obtained. While maintaining the basic elements of the source and environment of the WTS-4 machine, we introduce restrictions which simplify the ray path equation and allow its use with the computer program

68

MEDUSA. The results of the applications of MEDUSA, in particular propagation loss curves, are compared to Willshire's data. Good agreement is obtained. Because of the visualization of the sound field provided by ray theory, we have been able to interpret the downwind sound field as being that of a near-ground sound channel.

Furthermore, we describe Willshire's follow-up experiments conducted during May-June 1985. Both upwind and downwind measurements were made. In contrast to the September experiments, which yielded a 4 hour time average of the field, the May-June 1985 experiments provided simultaneous measurements of the sound field. Again, we compare ray theory predictions to the data. Although more scatter is seen in the data from the second experiment, the data confirm the existence of the sound channel. In particular, our investigation correctly predicts the position and the magnitude of the jump in the sound level associated with the onset of multiple ray arrivals.

7.2 Upwind Sound Field

The goal of this thesis is to provide a theoretical basis with which to explain the downwind sound levels as measured by W. L. Willshire. However, Willshire also made upwind measurements. We have applied our theory, with modification to account for upwind propagation, to Willshire's data. We have found that ray theory cannot accurately be applied to the upwind sound field. Although Willshire's measurements show that the upwind sound field has drastically lower sound levels compared to the downwind field, the ray theory results predict a complete absence of sound beyond a distance of only 200 m, i.e., a shadow zone. Willshire's measurements clearly indicate that a shadow zone does not form.

7.3 Comments

Why does ray theory work well for the downwind sound field but not the upwind field? Because our investigation deals with simple propagation from a spherical source above a reflecting boundary, the formation of caustics is the most serious threat to the successful application of ray theory. Although caustics form downwind, they are too far away to affect the field near the ground. However, the formation of a caustic surface, i.e., a shadow zone, in the upwind direction proves fatal for ray theory.

In conclusion, we have found that ray theory, despite the initial uncertainty about its application at such low frequencies, is a good predictor of the basic features of the downwind sound field. In contrast, ray theory is not a good predictor of the upwind sound field.

7.4 Further Investigations

The inclusion of caustic corrections with ray theory could provide a substantial improvement over simple ray theory. We have stated in Appendix D that we expect caustic corrections to smooth the PL curve in the downwind direction. In contrast a shadow zone is expected, based on simple ray theory, to form in the upwind direction. However, it is known that sound penetrates the shadow zone [4]. An interesting test of the utility of caustic corrections would be the ability to account for the shadow zone field.

Sound propagation in directions away from the upwind-downwind axis has not been considered. In directions away from directly downwind, propagation could be handled by considering the following simple approximation. The net effect of the wind velocity on sound propagating in the direction perpendicular

70

to the upwind-downwind axis (at $\pm 90°$ to the axis) is simply to 'carry' the sound downwind, i.e., no refraction occurs for propagation in the 90° direction (see for example Ref. 28). At intermediate angles the refraction effects of the wind can be added through a $\cos \alpha$ term where α is the angle away from the downwind direction. Consequently the propagation speed becomes

$$c = c_0 + w \cos \theta \cos \alpha \quad , \tag{7.1}$$

where α takes on values from 0° to 90°. The PL curves for a suitable set of angles between $\alpha = 0°$ and $\alpha = 90°$ could be computed separately in the manner described in this thesis with the the propagation speed given by Eq. (7.1). The results for each α could be assembled to give a plan view of the sound field. In the case of the WTS-4 machine corrections would have to be added to account for the dipole nature of the source. Furthermore, we have assumed that temperature has no effect on propagation, but as the effect of the wind velocity descreases to zero, temperature effects, however small, would have to be incorporated.

APPENDIX A

Ground Wave Effects

During his initial analysis of the WTS-4 data from the September 1984 experiment, Willshire's interest centered on the role played by the so-called ground wave. In this appendix ground wave theory is summarized. We also reproduce the evidence that led Willshire to conclude that the ground wave effect was unimportant in the downwind sound field. The discussion in this appendix is taken mainly from Refs. 4 and 29. A detailed development of the following can also be found in Ref. 19.

A.1 The Ground Wave

As noted in Section 1.4, we neglected a term in the expression for the sound radiated from a source near the ground. Here we include that term:

$$
\begin{aligned}
\frac{p}{p_0} &= (\frac{1}{r_1})e^{-ikr_1} + (\frac{R_p}{r_2})e^{-ikr_2} \\
&\quad + (1 - R_p)(\frac{F}{r_2})e^{-ikr_2} \quad ,
\end{aligned}
\tag{A.1}
$$

where F is an amplitude factor (see Eq. (2), Ref. 29). The first term represents the direct wave, the second term the reflected wave, and the third term what is

called the ground wave.[1] As the angle of incidence (ψ in Fig. 1.3) nears 0, R_p nears -1, and the incident and reflected waves cancel. The ground wave then becomes the only contribution to the sound field.

A.2 Surface Wave Contributions

The picture is further complicated in the general case where the ground impedance is complex. When the source and receiver are both above the ground the complete field may be expressed in words as

$$\frac{p}{p_0} = \text{direct wave}(r^{-1}) + \text{reflected wave}(r^{-1})$$
$$+\text{ground wave}(r^{-1}) + \text{surface wave}(r^{-1/2}) \quad , \qquad (A.2)$$

where the terms in parentheses indicate the functional dependence on range. Note that the third term of Eq. (A.1) has split into two terms, each with a distinctly different dependence on range. At long range and with the source near the ground, it is clear that the major contribution to the sound field is the surface wave. This is the component of the sound field with which Willshire was initially interested. The $r^{-1/2}$ dependence coincides with the cylindrical spreading behavior observed.

Figure A.1 shows Willshire's comparison between his field measurements and the predicted levels based on ground wave theory. From the comparison, Willshire concluded that the ground wave could not be the primary factor causing the downwind sound field to follow cylindrical spreading, rather than a spherical spreading curve.

Although it turned out that the ground wave was not of primary importance in the propagation of downwind noise, the ground wave is of interest in

---

[1] The term 'ground wave' derives from the analogous problem in electromagnetics (in Ref. 4, Piercy et al. point out that the electromagnetic ground wave is the vehicle of transmission for local AM radio stations).
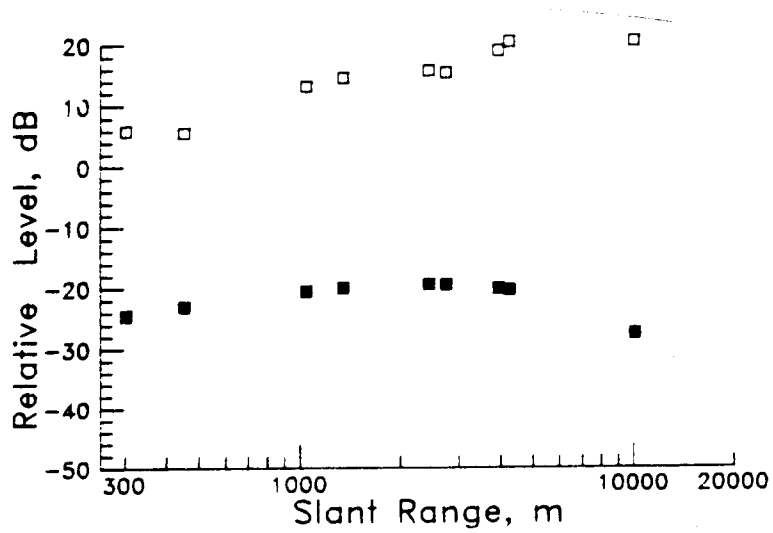
Figure A.1 COMPARISON OF PREDICTED GROUND WAVE LEVELS AND WILLSHIRE'S DATA. SOLID SQUARES ARE THE PREDICTED LEVELS AND THE EMPTY SQUARES ARE THE MEASURED LEVELS.

outdoor acoustics. In fact, it may play a sensible role in upwind propagation.

APPENDIX B

Beam Displacement

B.1 Introduction

Beam displacement has been shown to be an important way to extend the usefulness of ray theory. For example, Tindle and Bold [30] have successfully studied problems which are usually treated with normal mode theory because of the frequency limitations of ray theory. With this in mind we investigated the feasibility of using beam displacement in studying the propagation of low frequency sound from wind turbines.

B.2 The Head Wave and Beam Displacement

Beam displacement is a phenomenom associated with total internal reflection. Recall that the reflection coefficient R for a ray incident on a plane surface is given by

$$R = \frac{Z_{ground} \cos \psi_i - Z_{air} \cos \psi_t}{Z_{ground} \cos \psi_i + Z_{ground} \cos \psi_t} \quad , \tag{B.1}$$

where Z_{air} and Z_{ground} are the impedances of air and ground, respectively, and ψ_i and ψ_t are the angles measured with respect to the normal to the interface,
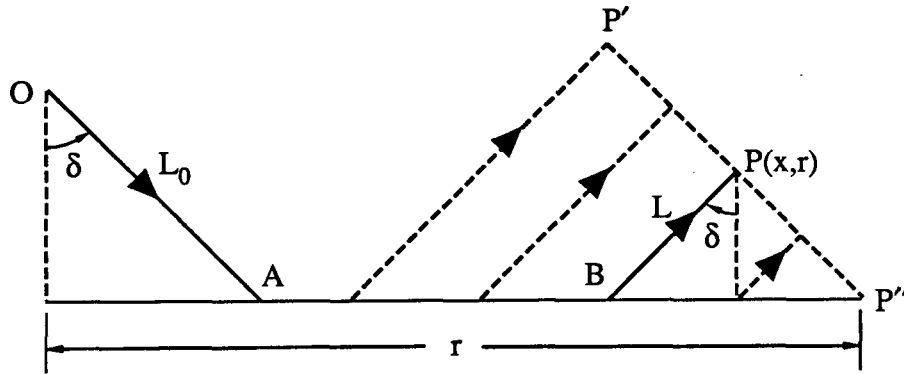
Figure B.1 SOUND FIELD FROM A HEAD WAVE.

of the incident and transmitted rays, respectively (in contrast to Eq. 1.5 which includes the grazing angle). The critical angle is defined as

$$\delta = \sin^{-1}(c_{air}/c_{ground}) \quad , \tag{B.2}$$

where c_{air} and c_{ground} are the sound speeds in air and in the ground, respectively. If the angle of incidence is less than the critical angle, $\psi_i < \delta$, normal reflection and refraction occur. If $\psi_i = \delta$, the transmitted wave travels along the air-ground interface. If $\psi_i > \delta$, total internal reflection is said to have occurred.

A simple understanding of beam displacement may be gained by considering Fig. B.1. Note the ray OA whose angle of incidence is $\psi_i = \delta$. No transmitted ray occurs in this case. Furthermore, a wave continues along the interface AB and continually reradiates into the upper medium as it propagates. The continual reradiation contributes to the wavefront $P'P''$. This wavefront is called the *head wave* or *lateral wave*. If an observer is located at $P(x, r)$ he will measure a ray $OABP$ which has been displaced an amount AB. A cluster of

76
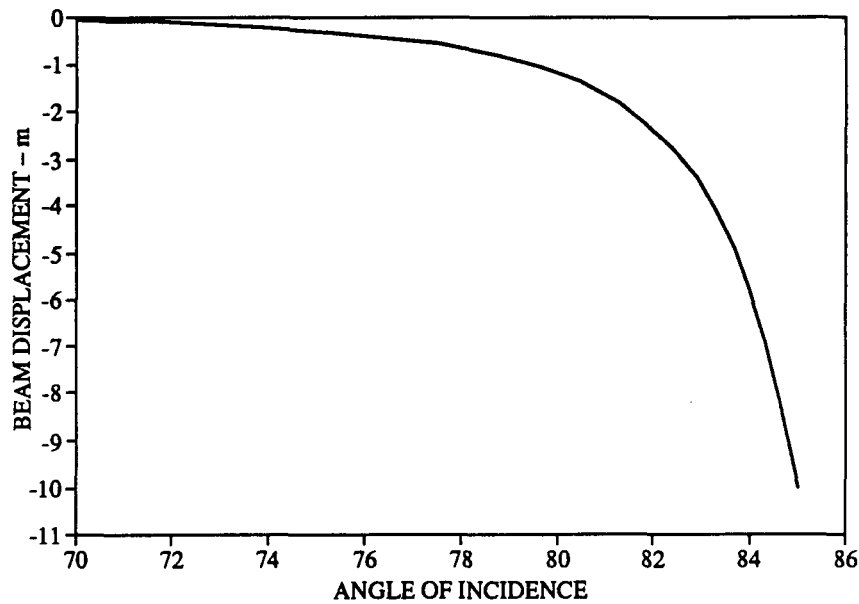
Figure B.2 BEAM DISPLACEMENT AS A FUNCTION OF THE ANGLE OF INCIDENCE.

rays near critical incidence will form a beam whose center will be displaced a similar amount, and hence the term *beam displacement*. A good review of beam displacement is found in Ref. 32.

Given the angle of incidence and certain properties of the source and environment, we can explicitly calculate beam displacement. Using a program designed by E. K. Westwood [31], we made detailed calculations to determine the effect of beam displacement in the propagation of sound from the WTS-4 wind turbine. Figure B.2 shows a computer generated plot of beam displacement versus the angle of incidence for a fan of rays undergoing a single reflection. The properties supplied to the program are the following: (1) the density of air, 0.001 kg/m^3, (2) the compressional wave speed in air, 343 m/s, (3) the shear wave speed in air (which of course is zero because shear waves do not propagate in air), (4) the density of dry ground, 1.922 kg/m^3, (5) the compressional wave speed for dry ground, 762 m/s, and (6) the shear wave speed for dry ground, 457 m/s. The

values for the ground properties are approximately those[1] of the ground near the wind turbine at Medicine Bow, Wyoming. They are not actual measurements from Medicine Bow, Wyoming. The beam displacement calculations were made for a frequency of 10 Hz and the propagation velocity profile, Eq. (3.2), described in Chapters 4 and 5 of this thesis. Figure B.2 indicates that beam displacement is negligible except for angles of incidence just under 90° (grazing angle less than 10°). In the downwind direction we deal with very shallow grazing angles. However, the rays are refracted downward. In fact, the grazing angle for incident rays at the ground is never less than 10° and increases with range. The results indicate that beam displacement is relatively unimportant in the downwind direction for low frequency sound. In the upwind direction rays can be incident at angles less than 10°. In this case, beam displacement may play a role. However, the dominant feature in the upwind direction is the shadow zone.

---

[1]These properties were supplied by Dr. K. H. Stokoe, Civil Engineering Department, The University of Texas at Austin.

APPENDIX C

MEDUSA

In this appendix, we provide a general overview of MEDUSA. Our description is a summary of Chapter VI of the technical report by T. L. Foreman [23]. Additionally, we describe a typical MEDUSA *run* used in our investigation.

The software package MEDUSA is in fact a collection of FORTRAN programs. Figure C.1 (Fig. 9 of Ref. 23) shows the overall organization of MEDUSA. The boxes contain the names of the separate programs. Input required for each program is indicated by arrows coming into the boxes and output by arrows leaving the boxes. A short description of the input, the programs, and their output is as follows.

RAYFAN solves the ray path equation and generates ray history records. The records may be output in tabular form. RAYFAN requires the sound speed profile, the source depth, the receiver depth, and bathymetry. The term bathymetry refers to the shape of an ocean bottom, a sloping bottom, for example. We did not use this feature. It could be useful, however, in investigating the role played by the topology of the WTS-4 site, for example, the atypical environment of the microphone at 10 km in the May-June 1985 experiment.

ENVPLT plots sound speed profiles and bathymetry. In addition, the sound speed profile and ocean bottom depth at each range can be plotted together.
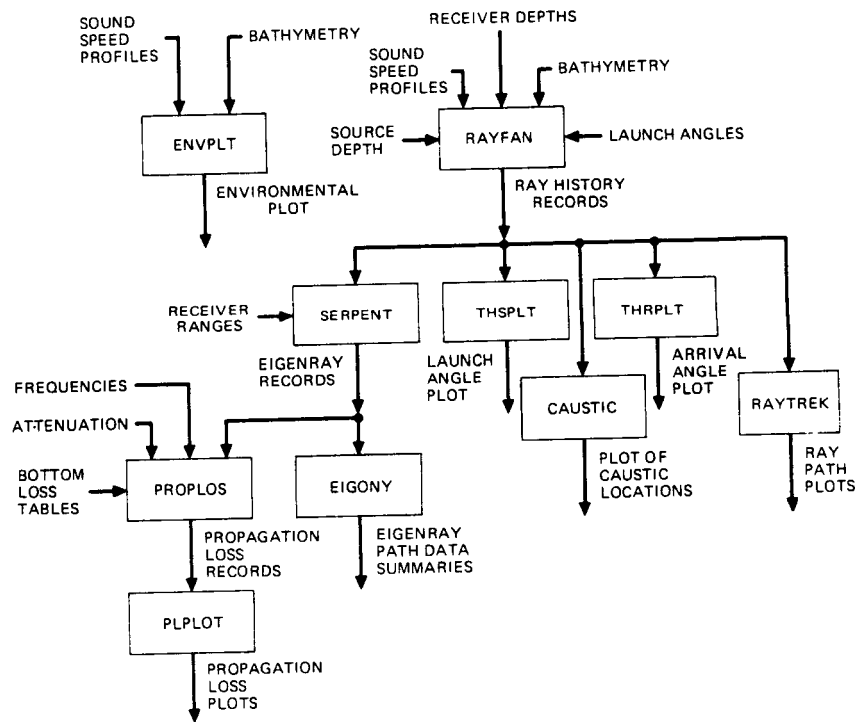
Figure C.1 ORGANIZATION OF MEDUSA.

Five programs use the ray history records as input. RAYTREK generates the ray plots. CAUSTIC plots the location of caustics. SERPENT locates the eigenrays from the ray history records generated by RAYFAN. THSPLT and THRPLT plot the launch angle and the arrival angle, respectively.

In Fig. C.1 we have retained the references to depth in the input. As noted in Chapter 3, we translated depth to height above the ground. In most cases the translation required a simple hand calculation. The single exception is the propagation speed. In our investigation the propagation speed is input to MEDUSA as a formula contained in a subroutine. In this instance, the translation of depth to height was included in the subroutine.

After the input file is built, a typical MEDUSA run conducted during our investigation proceeds in the following manner.

- Ray plots. To get ray plots we ran RAYFAN for the desired launch angles and then ran RAYTREK to obtain the plots. It was necessary to modify the plotting routines so that 'height' is plotted instead of depth.

- Caustic plots. Caustic plots were obtained in much the same way as ray plots. However, RAYFAN had to be run with a large number of rays in order to find as many caustics as possible. Again, the plotting routines were modified to display 'height' instead of 'depth.'

- PL plots. To obtain PL plots it was necessary to run three programs. SERPENT was run to locate eigenrays, then PROPLOS computed propagation loss, and finally, PLPLOT plotted the output of PROPLOS. It was not necessary to modify the plotting routines of PROPLOS. However, a spherical spreading curve was added for the purposes of this investigation. We note here that although MEDUSA does not include caustic corrections in com-

puting the propagation loss, it does include the $\pi/2$ phase shift associated with the passage of a ray through a caustic.

APPENDIX D

The Effect of Caustics on Sound Intensity

In the investigation of sound propagation from the WTS-4 wind turbine we have, as a first approximation, assumed that caustics need not be accounted for when calculating the PL curve. As we have seen, ignoring caustics has yielded good results. However, caustics do occur in the sound field and it is appropriate that a description of caustics be included in this thesis. Here, we give a qualitative description of caustics and their effect on the sound field.

D.1 The Formation of Caustics

A qualitative picture of what caustics are and how they are formed is now provided. Consider a portion of a wavefront between two closely spaced rays associated with the wavefront (see Fig. D.1). The two rays define a *ray tube*, the cross-sectional area of which varies as the wave propagates. If the sound in the ray tube does not leak out, the sound intensity I at any field point must be inversely proportional to the ray tube area A. In terms of the focusing factor I/I_0, where I_0 is the source intensity, the proportionality is

$$\frac{I}{I_0} \propto \left(\frac{A_o}{A} \right) \quad ,$$
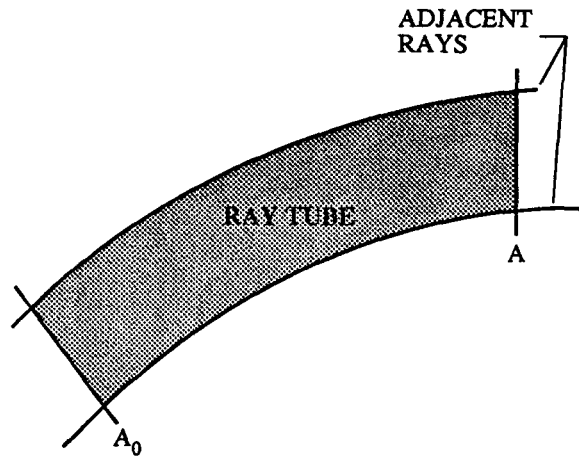
Figure D.1 Ray tube formed by closely spaced rays.

where A_o is the area of the ray tube at the source. If the rays are refracted in such a way that they cross, the area A goes to zero, the focusing factor goes to infinity, and the propagation loss becomes undefined. The envelope of crossings of adjacent rays is called a *caustic surface,* or simply a *caustic.*

It is important to keep in mind that a caustic is not an aberrant physical phenomenon, but simply the focusing of rays (in fact, an ordinary point focus produced by a lens is a special case in which the caustic is a single point [33]). On the other hand, it is apparent why caustics are a problem: the intensity of sound at caustics clearly cannot go to infinity as predicted with simple ray theory. Ray theory must therefore be modified (or abandoned) near caustics if the sound intensity is to be calculated there.

Besides preventing (locally) the accurate calculation of propagation loss, the rapid increase of sound intensity near a caustic violates a basic assumption of ray theory: the amplitude of the sound wave should not vary drastically over a wavelength. Thus a region exists near a caustic where ray theory is inapplicable. However, caustic effects are of local importance only in the sense that away from

84

the caustic, simple ray theory is once again valid.[1] Consequently, even though they occur in a sound field, caustics can be ignored, *provided* the receiver is not near a caustic.

D.2 Airy Function

However, caustics do form. If caustics form and they cannot be ignored, ray theory can still be salvaged by modifying its sound intensity calculation scheme. That is, an approximate formula for the sound intensity exists which is well behaved at the caustic, and which returns to the simple ray theory formula away from the caustic. The solution is described qualitatively in the remainder of this section (a rigorous derivation is beyond the scope of this thesis).

As an introduction to the approximate solution, we present a doctored passage from Ref. 33. Phenomena that occur which cannot be accounted for with ray theory are called *diffraction phenomena*, of which caustics are an example. In Ref. 33 Landau and Lifshitz describe the problem of the diffraction of electromagnetic waves caused by an opaque object. Nevertheless, the passage applies equally well to diffraction of acoustic waves, and to emphasize the fact we have changed a few phrases (italicized words) to make the passage applicable to acoustics.

> The problem of the theory of diffraction consists in determining, for
> given positions and shapes of the objects (and locations of the *sound*
> sources), the distribution of the *sound,* that is, the *acoustic* field over
> all space. The exact solution of this problem is possible only through

---

[1]Permanent phase change is an exception to this generalization. If a ray is tangent to a caustic, the signal associated with the ray undergoes a phase change [33]. This is a comparatively simple problem and, in fact, the program MEDUSA accounts for the phase change. The primary problem here is the correct calculation of intensity, which MEDUSA cannot provide at or near a caustic.

solution of the wave equation with suitable boundary conditions at the surface of the body, these conditions being determined also by the *acoustical* properties of the material. Such a solution usually presents great mathematical difficulties.

However, there is an approximate method which for many cases is a satisfactory solution of the problem of the distribution of *sound* near the boundary between *insonified region* and *shadow zone*. This method is applicable to cases of small deviation from *geometrical acoustics*, i.e., when firstly, the dimensions of all bodies are large compared with the wavelength ... ; and secondly when there are only small deviations of the *sound waves* from the directions of the rays given by *geometrical acoustics*.

In the following paragraphs we comment on the terms *insonified region* and *shadow zone*.

Using *Huygen's principle* (the method referred to in the above quotation), Landau and Lifshitz find that the intensity is proportional to the square of the *Airy function*. Derivations more familiar to acousticians can be found in acoustics textbooks [32,10]. The intensity near a caustic is given approximately by the formula

$$I \propto \text{Ai}^2(\eta) \quad ,$$

where

$$\eta = -y \left(\frac{2k^2}{R_c} \right)^{1/3} \quad ,$$

$\text{Ai}(\eta)$ is the *Airy function*, η is a nondimensional function of the radius of curvature R_c of the caustic, the wave number k, and the distance from the caustic y. The explicit formula for the intensity is not our primary concern here. In
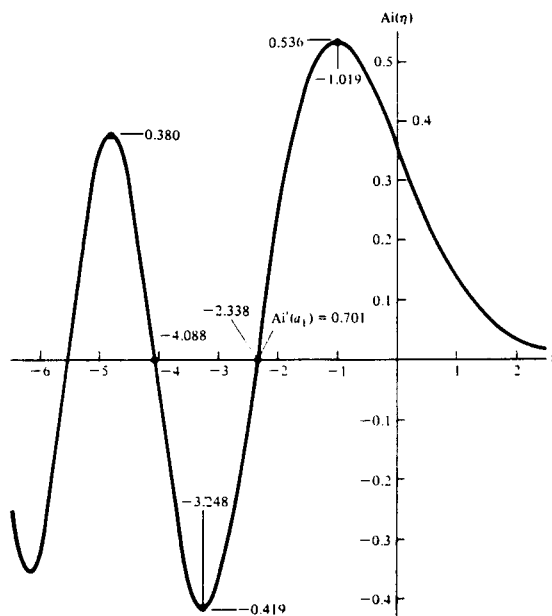
Figure D.2 PLOT OF THE AIRY FUNCTION (FROM REF. 10).

fact, the formula varies somewhat depending on the method of derivation (see, for example, Section 9-4 of Ref. 10). More important is the behavior of the Airy function. Figure D.2 is a reproduction of a plot of the Airy function Ai(η) taken from Ref. 10. Note that the Airy function is asymmetrical about $\eta = 0$ (the position of the caustic). In the *shadow zone* ($\eta > 0$) the Airy function goes to zero exponentially, while in the *insonified zone,* ($\eta < -1$) the Airy function is oscillatory. The simple ray theory formula for intensity is recovered [34] well inside the insonified region. Use of the Airy function avoids the the catastrophe at the caustic and provides a smooth variation of the intensity from the insonified region to the shadow zone.

A qualitative understanding of the physics behind the Airy function may be obtained from consideration of Fig. D.3. In this figure we have redrawn the Airy function with a caustic surface and two rays which graze the surface (recall the phase change associated with grazing or passing through the surface). Note
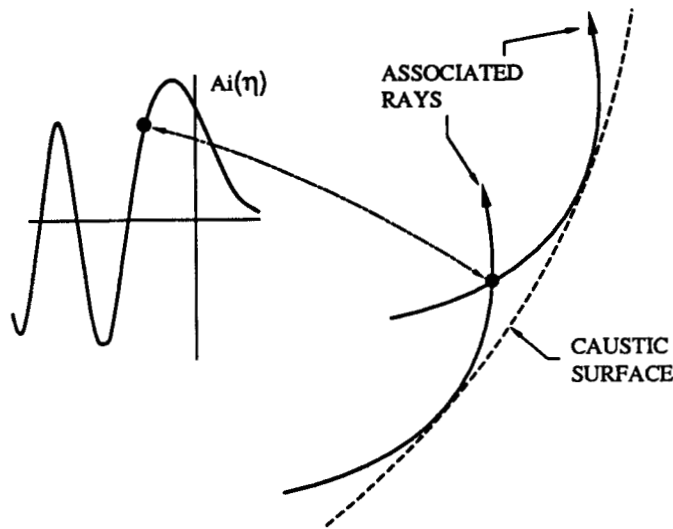
Figure D.3 PLOT OF THE AIRY FUNCTION WITH ASSOCIATED RAYS NEAR A CAUSTIC SURFACE.

that the rays intersect near the caustic surface. Depending on the phase, the sound associated with each ray can add either constructively or destructively. Consequently, the intensity has an oscillatory behavior near the caustic surface given by the Airy function.

In summary, our first approximation is to ignore caustics completely (except for the phase change) and use simple ray theory to calculate intensity. If, however, the receiver is near a caustic, the correction described above may be used to obtain an accurate calculation of the propagation loss.

APPENDIX E

MID-FREQUENCY SOUND LEVELS

In Chapter 5 we noted that Willshire's 1984 experiment included a few mid-frequency measurements. Here we present PL curves for two mid-frequency components and include ray diagrams which demonstrate the effect of raising the source height.

Figures E.1 and E.2 show the propagation loss for 63 and 250 Hz. The properties supplied to the input data file are the same as those described in Chapters 4 and 5. The exception is the source height, which is taken to be 120 m. The source is raised because, as we have stated in Chapter 2, the source of the high frequency noise is considered to be located near the top of the turbine.

The 1984 measurements made by Willshire at the WTS-4 wind turbine site show that the sound level drops off spherically for ranges up to 1200 m (in contrast, the low frequency measurements are significantly above spherical spreading). We see good agreement between ray theory predictions and Willshire's data. Note that ray theory predictions again include downrange channeling. However, the sound channel begins much farther downrange than in the case for a source located 40 m off the ground. Unfortunately, experimental data are not available for ranges beyound 1200 m.

C - 2
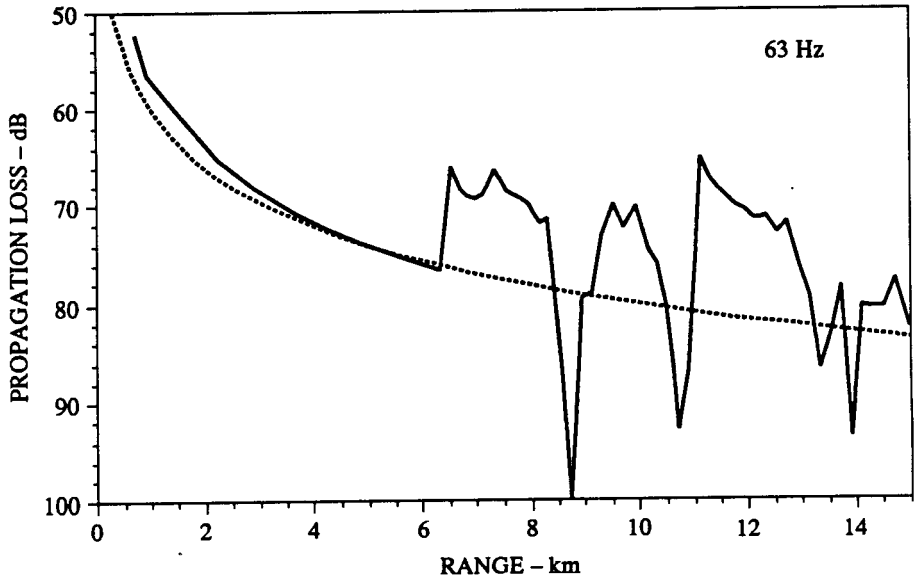
Figure E.1 PROPAGATION LOSS AT 63 Hz.
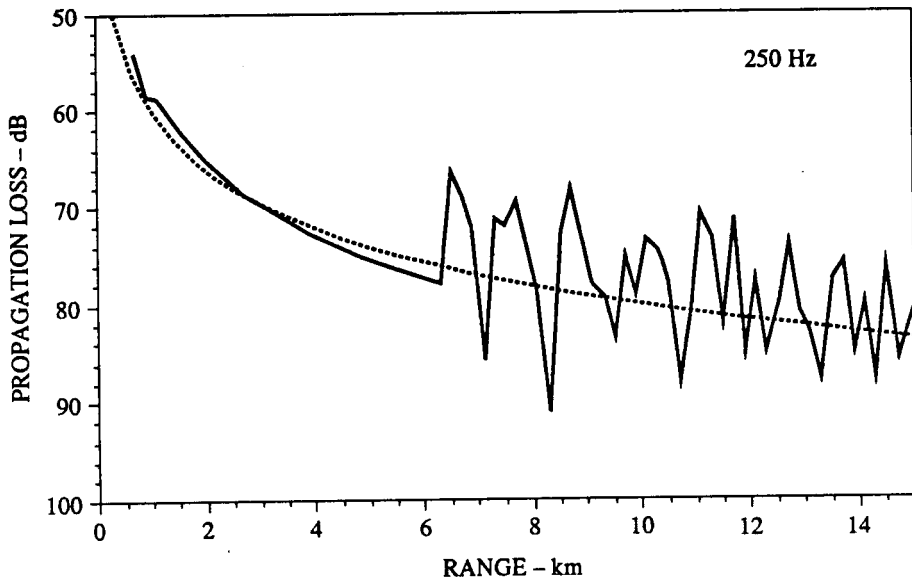
Figure E.2 PROPAGATION LOSS AT 250 Hz.

90

Figures E.3 and E.4 show a family of rays with a source at 120 m and 80 m, respectively. From these figures, we can see that the sound channel begins farther downrange as the source height is raised. For the 80 m source, the onset of multiply reflected rays begins between 4.3 and 4.5 km. For the 120 m source, the multiply reflected rays begin between 6.2 and 6.8 km. Willshire first suspected that a higher source height for the mid-frequency components could result in the levels staying nearer spherical spreading (see Fig. 11 in Ref. 5). Here, we have confirmed his conjecture that a higher source height results in an extended spherical spreading region.

In the channel region, the PL curve is much more jagged and generally closer to the spherical spreading curve than in the low frequency case. Two possible explanations are the following: (1) because of the higher frequencies, there is more interference, and (2) at higher frequencies the ground is more reactive and concommitantly more absorbent. This behavior is puzzling because ray theory is generally believed to work better at higher frequencies. The explanation of propagation loss behavior is a suitable subject for future investigations.
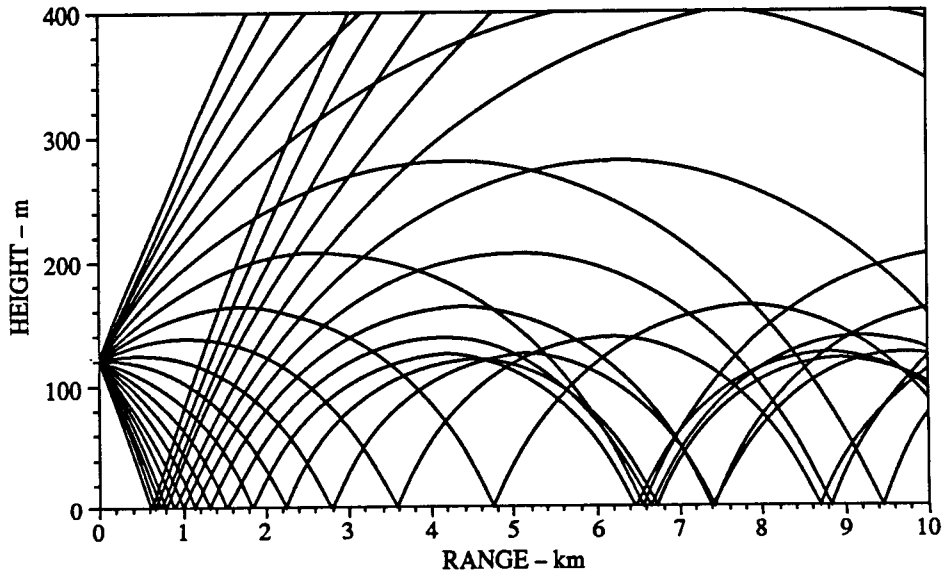
Figure E.3 FAMILY OF RAYS WITH SOURCE HEIGHT 120 M.
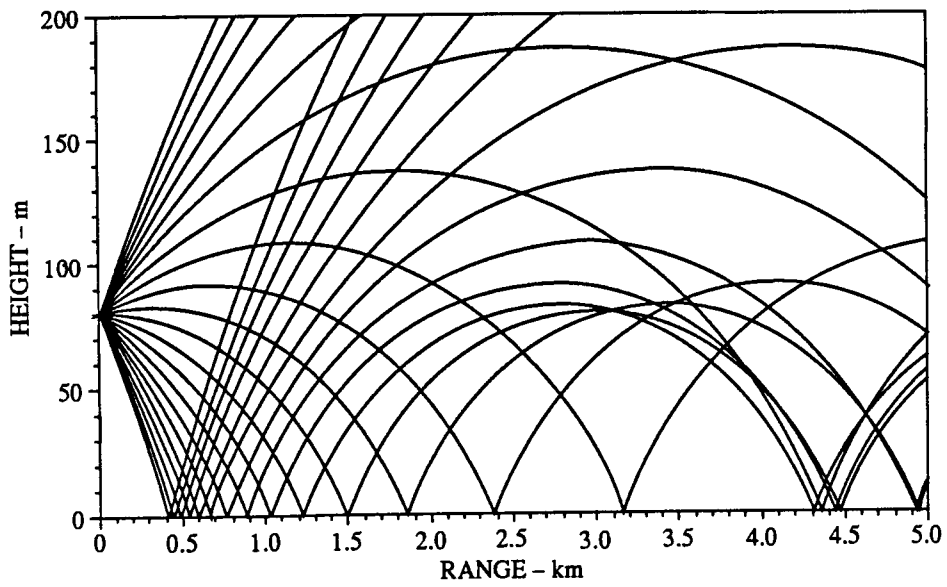
Figure E.4 FAMILY OF RAYS WITH SOURCE HEIGHT 80 M.

92

REFERENCES

[1] P. M. Moretti and L. V. Divone, "Modern windmills," *Scientific American* **254**, 110–118 (1986).

[2] H. H. Hubbard, F. W. Grosveld, and K. P. Shepherd, "Noise characteristics of large wind turbine generators," *Noise Control Engineering Journal* **21**(1), 21–29 (1983).

[3] N. D. Kelley, "Acoustic noise production by the DOE/NASA MOD-1 wind turbine," presented at Wind Turbine Dynamics Conference, Cleveland, Ohio, NASA Conference Publication 2185, 1981.

[4] J. E. Piercy, T. F. Embleton, and L. C. Sutherland, "Review of noise propagation in the atmosphere," *J. Acoust. Soc. Am.* **61**, 1403–1418 (1977).

[5] W. L. Willshire, "Long range downwind propagation of low-frequency sound," NASA TM 86409, April 1985.

[6] I. P. Chunchuzov, "Review of noise propagation in the atmosphere," *J. Acoust. Soc. Am.* **58**, 1403–1418 (1985).

[7] W. E. Zorumski and W. L. Willshire, "Propagation of normal acoustic modes in an atmospheric boundary layer," *J. Acoust. Soc. Am.* **80**, S19 (A) (1986).

[8] F. D. Tappert, "The parabolic approximation method," Chapter 3 in *Wave Propagation and Underwater Acoustics*, edited by J. B. Keller and J. S. Papadakis (Springer-Verlag, New York, 1977), 224–287.

[9] M. J. White and K. E. Gilbert, "Application of the parabolic wave equation to atmospheric sound propagation over a locally reacting ground surface," *J. Acoust. Soc. Am.* **80**, S20(A) (1986).

[10] A. D. Pierce, *Acoustics* (McGraw-Hill Book Company Inc., New York, 1981).

[11] M. E. Delany, "Sound propagation in the atmosphere: a historical review," *Acustica* **38**, 201–223 (1977).

[12] E. H. Brown and F. F. Hall, Jr., "Advances in atmospheric acoustics," *Review of Geophysics and Space Physics* **16**, 47–110 (1978).

[13] R. B. Lindsay, *Mechanical Radiation* (McGraw-Hill Book Co., Inc., New York, 1960).

[14] L. E. Kinsler, A. R. Frey, A. B. Coppens, and J. V. Sanders, *Fundamentals of Acoustics* (John Wiley & Sons, New York, 1982).

[15] I. Rudnick, "Propagation of sound in air," *Handbook of Noise Control*, edited by C. M. Harris, (McGraw-Hill Book Co., New York, 1957), pp. 3-1 to 3-17.

[16] K. P. Shepherd and H. H. Hubbard, "Measurements and observations of noise from a 4.2 megawatt (WTS-4) wind turbine," NASA Contractor Report 166124 (May 1983).

[17] A. Miller, *Meterorology*, (Charles E. Merrill Publishing Company, Columbus, Ohio, 1976).

[18] M. E. Delaney and E. N. Bazley, "Acoustical properties of fibrous absorbent materials," *Appl. Acoust.* **3**, 105–116 (1970).

[19] C. I. Chessel, "Propagation of noise along an impedance boundary," *J. Acoust. Soc. Am.* **62**, 825–834 (1977).

[20] D. G. Stephens, K. P. Shepherd, H. H. Hubbard, and F. W. Grosveld, "Guide to the evaluation of human exposure to noise large wind turbines," NASA TM 83288 (March 1982).

[21] S. A. L. Glegg, "Noise from wind turbines," Paper J3-6, in the *Proceedings of the 12th International Congress of Acoustics*, 24-31 July 1986, Volume III.

[22] J. Lighthill, *Waves in Fluids* (Cambridge University Press, New York, 1980).

[23] T. L. Foreman, "Ray modeling methods for range dependent ocean environments," Applied Research Laboratories Technical Report No. 83-41 (ARL-TR-83-41) Applied Research Laboratories, The University of Texas at Austin (1983) (ADA-137202).

[24] W. L. Willshire, Jr., "Long-range downwind propagation of low-frequency noise," *J. Acoust. Soc. Am.* **77**, S1(A) (1985).

[25] L. D. Landau, and E. M. Lifshitz, *Fluids Mechanics* (Pergamon Press, Oxford, 1959).

[26] R. J. Urick, *Principles of Underwater Sound* (McGraw-Hill Book Co., Inc., St. Louis, 1975).

[27] H. H. Hubbard, K. E. Shepherd, and W. L. Willshire, "Results of simultaneous acoustic measurements around a large horizontal axis wind turbine," *J. Acoust. Soc. Am.* **80**, S28(A) (1986).

[28] K. U. Ingard, "Review on the influence of meteorlogical conditions on sound propagation," in *Proceedings of the Fourth Annual Noise Abatement Symposium* (publisher unknown, 1955), 11–25.

[29] T. F. Embleton, J. E. Piercy, and N. Olson, "Outdoor sound propagation over ground of finite impedance," *J. Acoust. Soc. Am.* **59**, 825–834 (1977).

[30] C. T. Tindle and G. E. J. Bold, "Improved ray calculations in shallow water," *J. Acoust. Soc. Am.* **70**, 813–819 (1981).

[31] E. K. Westwood and C. T. Tindle, "Shallow Water Time Series Simulation Using Ray Theory," *J. Acoust. Soc. Am.* **81**, 1752–1761 (1987).

[32] L. M. Brekhovskikh and Yu. Lysanov, *Fundamentals of Ocean Acoustics* (Springer-Verlag, Berlin, 1982).

[33] L. D. Landau and E. M. Lifshitz, *The Classical Theory of Fields* (Pergamon Press, Oxford, 1975).

[34] R. Pitre, "On the application of horizontal ray theory to acoustic propagation in the ocean waveguide," Applied Research Laboratories Technical Report No. 84-1 (ARL-TR-84-1), Applied Research Laboratories, The University of Texas at Austin (1984) (ADA 143 944).

Standard Bibliographic Page

1. Report No. NASA CR-178367	2. Government Accession No.	3. Recipient's Catalog No.
4. Title and Subtitle APPLICATION OF RAY THEORY TO PROPAGATION OF LOW-FREQUENCY NOISE FROM WIND TURBINES		5. Report Date July 1987
		6. Performing Organization Code
7. Author(s) James A. Hawkins		8. Performing Organization Report No. ARL-TR-87-40
9. Performing Organization Name and Address Applied Research Laboratories The University of Texas at Austin P. O. Box 8029 Austin, TX 78713-8029		10. Work Unit No. 505-61-11-02
		11. Contract or Grant No. NAS1-17802
12. Sponsoring Agency Name and Address National Aeronautics and Space Administration Langley Research Center Hampton, VA 23665-5225		13. Type of Report and Period Covered Contractor Report
		14. Sponsoring Agency Code

16. Abstract

   Ray theory has been used to explain data from two experiments, done in 1984 and 1985, on propagation of low frequency sound generated by the WTS-4 wind turbine located in Medicine Bow, Wyoming. Emphasis is on downwind data, but some upwind measurements taken during the 1985 experiment are also considered. In this report, general ray theory for a moving medium is reviewed and the ray equations are obtained. Restrictions are introduced that simplify the equations and allow the use of a ray theory program MEDUSA. The results are then compared to the data. In particular, the MEDUSA computed propagation loss curve is compared to the measurements. Good qualitative agreement is obtained with downwind data from the 1984 experiment. The results indicate that the downwind sound field is that of a near-ground sound channel. Although more scatter is seen in the 1985 data, agreement between theory and the data is also good. In particular, the position and magnitude of the jump in the sound levels associated with the beginning of the sound channel is correctly predicted. The theoretical explanation of the upwind data is less successful. Ray theory calculations indicate the formation of a shadow zone that, in fact, does not occur. While no sharp shadow zone is apparent in the data, the general expectation (based on ray theory) that the sound levels should be much reduced upwind is confirmed by the data.

17. Key Words (Suggested by Authors(s)) Propagation speed gradient Propagation loss Atmospheric acoustics WTS-4 wind turbine Ray equations MEDUSA Ray paths Caustics	18. Distribution Statement Unclassified - Unlimited Subject Category 71

19. Security Classif.(of this report) Unclassified	20. Security Classif.(of this page) Unclassified	21. No. of Pages 105	22. Price A06